NASA TM X- *65921*

ACOUSTIC RESPONSE COMPARISON FOR A SPACECRAFT TESTED WITH AND WITHOUT A SHROUD
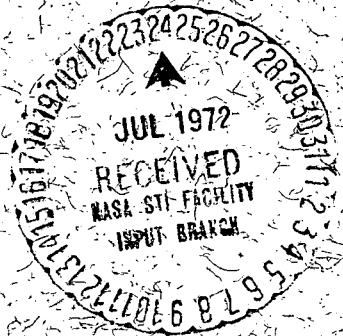
LLOYD R. BRUCK

FEBRUARY 1972

GSFC —— GODDARD SPACE FLIGHT CENTER ——
GREENBELT, MARYLAND

ACOUSTIC RESPONSE COMPARISON FOR A SPACECRAFT TESTED

WITH AND WITHOUT A SHROUD
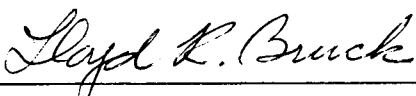
by

Lloyd R. Bruck
Goddard Space Flight Center

February 1972
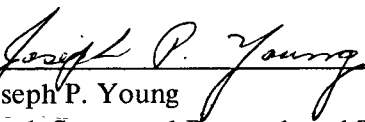
GODDARD SPACE FLIGHT CENTER
Greenbelt, Maryland

ACOUSTIC RESPONSE COMPARISON FOR
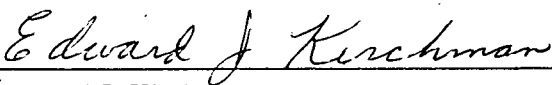A SPACECRAFT TESTED WITH AND
WITHOUT A SHROUD

Prepared by:

Lloyd R. Bruck
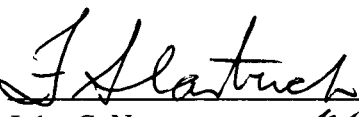Structural Research and Technology Section

Reviewed by:

Joseph P. Young
Head, Structural Research and Technology Section

Edward J. Kirchman
Head, Structural Dynamics Branch

Approved by:

John C. New
Chief, Test and Evaluation Division

FOREWORD

The work described within this report was performed under research task RTOP-124-08-14. The primary objective of this program is to advance the state of the art for the prediction and test simulation of the launch dynamic environment. This report is limited to discussing only one phase of the total test program—that of comparing the acoustic responses of a spacecraft with and without a shroud. An additional report, Lloyd R. Bruck: "Response of a Shroud-enclosed Spacecraft to Combined Acoustic-vacuum Environments," GSFC Document X-320-71-518, February 1972, presents the results of combined vacuum-acoustic tests.

ABSTRACT

For the purpose of evaluating the simulation problems encountered in an acoustic environment laboratory, a research test program using the Launch Phase Simulator was initiated. The Orbiting Geophysical Observatory (OGO) structural model and the Nimbus-type shroud were used as test items.

This report compares the acoustic vibratory response of the OGO model when enclosed within a shroud with the OGO acoustical response with the shroud removed, while subjected to an equivalent acoustic environment. The results indicate that a shroud is necessary in order to perform a realistic acoustic test. Tests with the shroud removed generate significantly lower spacecraft responses, and therefore are nonconservative.

To account for the significant effects the shroud removal can have on the response of the spacecraft to acoustic excitation, the complex relationships and interactions of the shroud on the spacecraft should be understood and properly simulated prior to conducting an acoustic test. These precautions must be observed if useful and applicable test data are to be gathered.

CONTENTS

ILLUSTRATIONS

TABLES

ACOUSTIC RESPONSE COMPARISON FOR
A SPACECRAFT TESTED WITH AND
WITHOUT A SHROUD

by

Lloyd R. Bruck
Goddard Space Flight Center

INTRODUCTION

A research program has been initiated to develop improved acoustic test simulation techniques for shroud-enclosed spacecraft. As part of this program, a series of research acoustic tests has been conducted using the acoustic test capabilities of the Launch Phase Simulator (LPS). The structural model of the Orbiting Geophysical Observatory (OGO) and the Nimbus-type shroud were used as test items.

The primary purpose of these tests was to compare the spacecraft response with the shroud installed to the response with the shroud removed, in order to evaluate the differences and/or similarities between these two test approaches.

BACKGROUND

The random vibration environment in the majority of current shroud/spacecraft systems results from external random pressure fluctuations. During launch and low-speed flight, these fluctuations are caused by acoustic noise radiated from the rocket propulsion system, whereas during higher-speed portions of flight the pressure fluctuations are generated by unsteady aerodynamic flows over the vehicle.

These severe fluctuating pressure loads impinge upon the shroud/launch vehicle configuration and are transmitted to the spacecraft through two paths, an air path and a mechanical path, as illustrated in Figure 1. The mechanical path, consisting of the load-carrying members of the launch vehicle, shroud, and spacecraft adapter trusses, provides a structural path for the acoustic energy to follow. The air path is through the shroud and, hence, directly onto the spacecraft. In either case, the resulting spacecraft response is random vibration over a broad frequency spectrum.

If one considers the spacecraft response caused only by the energy transmitted through the air path and neglects for the moment the response caused by energy transmitted through the structural path, there are two possible methods for the acoustic testing of the spacecraft.
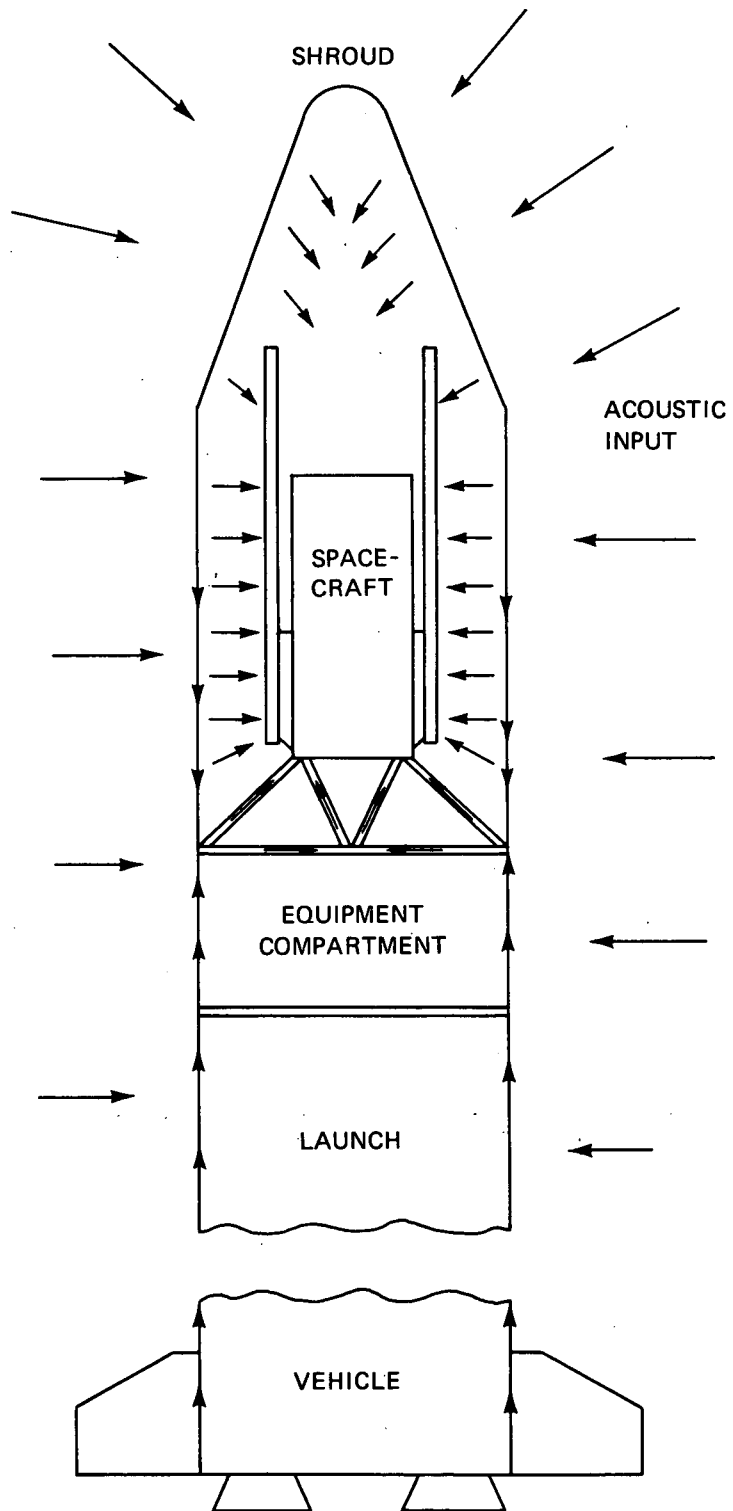
Figure 1. Transmission of Acoustic Energy to Spacecraft

One method is to subject the shroud/spacecraft combination to the predicted fluctuating pressure external to the spacecraft shroud. In the second method, the spacecraft alone is subjected to the predicted fluctuating pressures that would occur inside the shroud.

Even though there are two distinct methods to choose from, current practice has largely favored the method of testing with the spacecraft alone. There are several reasons why this approach is used: The obvious reasons relate to avoiding the expense and problems of having a shroud available and to decreasing the test configuration volume. A more subtle reason, but a much more important one, has been the belief that the direct acoustic excitation through the air path is the predominant cause of a spacecraft's high-frequency random response; therefore, eliminating the shroud and subsequent mechanical path should have a minimal effect on the spacecraft response.

TEST DESCRIPTION

Test Items

The OGO structural model and the Nimbus-type shroud (Figure 2) were used in the acoustic tests. Although the OGO model is structurally identical to the flight spacecraft, the total model mass represents only 71 percent of the flight-spacecraft mass. The primary difference between the model and the actual flight hardware is that many of the externally mounted dummy experiments and their supporting booms had been removed from the model and were no longer available.

The total weight of the flight spacecraft and experiments is about 476 kg (1050 lb). The central box structure, measuring 1.70 m × 0.78 m × 0.81 m (67 in. × 31 in. × 32 in.) is formed from lightweight, corrugated aluminum sandwich sheets. Four longerons in the corners of the spacecraft box, together with the side panels, are the basic load-carrying members. The acceleration and other flight loads are transmitted from the spacecraft to the launch vehicle via the longerons and adapter truss.

The solar arrays, mounted on a shaft passing through the main body, are shown (Figure 2) folded into the launch configuration. The total length of the spacecraft-truss package is 3.61 m (142 in.) from the base of the truss to the tip of the folded solar arrays.

The shroud is basically a ribbed cylindrical shell capped by a conical nose. Its diameter is 1.65 m (65 in.), and its total length is 5.66 m (223 in.). It is constructed of a glass-reinforced plastic laminate with aluminum hat-section stiffening rings spaced at various intervals within the shroud. The shroud is in two halves to permit separation in orbit; when installed, it is fastened by two explosive bolts at the base and by two bands along its length. A microquartz/felt thermal insulation blanket, 1.3 to 2.5 cm (1/2 to 1 in.) thick, is contained within the shroud.

Figure 3 details the shroud, spacecraft adapter truss, and spacecraft fixture interfaces for both the flight configuration and the test configuration. For a completely realistic flight simulation, it would have been more appropriate if the elastic properties of the launch-vehicle section represented by the test fixture had been taken into account rather than using a fixture that was relatively rigid. Because it was felt that the transmission of the high-

SHROUD

SOLAR ARRAYS

SPACECRAFT BOX

ADAPTER
TRUSS

RIGID
FIXTURE

RIGID
FIXTURE

LPS END CAP
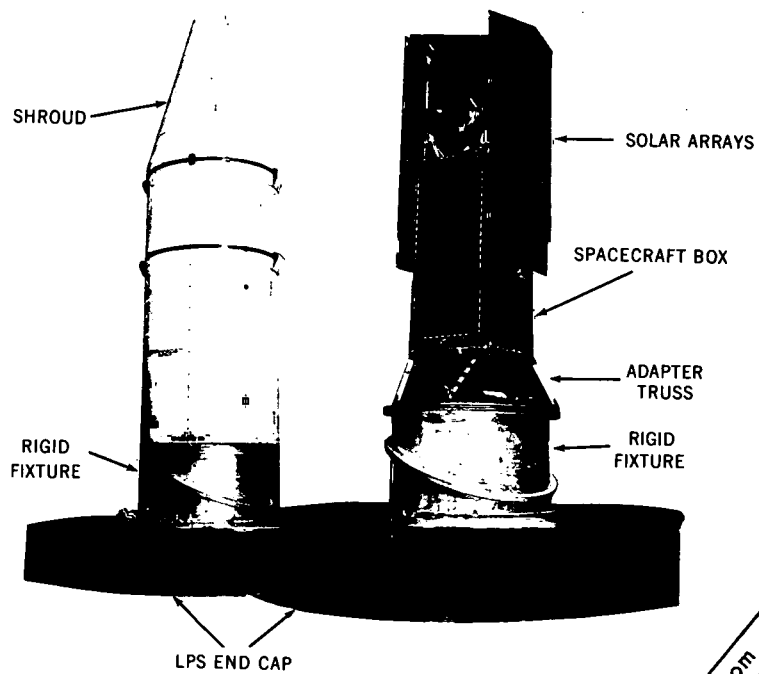
Figure 2. OGO Structural Model

SHROUD

ADAPTER TRUSS

ADAPTER TRUSS

SPACER

INTERFACE
RING

INTERFACE
RING

LAUNCH VEHICLE
MIDBODY SECTION

RIGID
FIXTURE

FLIGHT CONFIGURATION

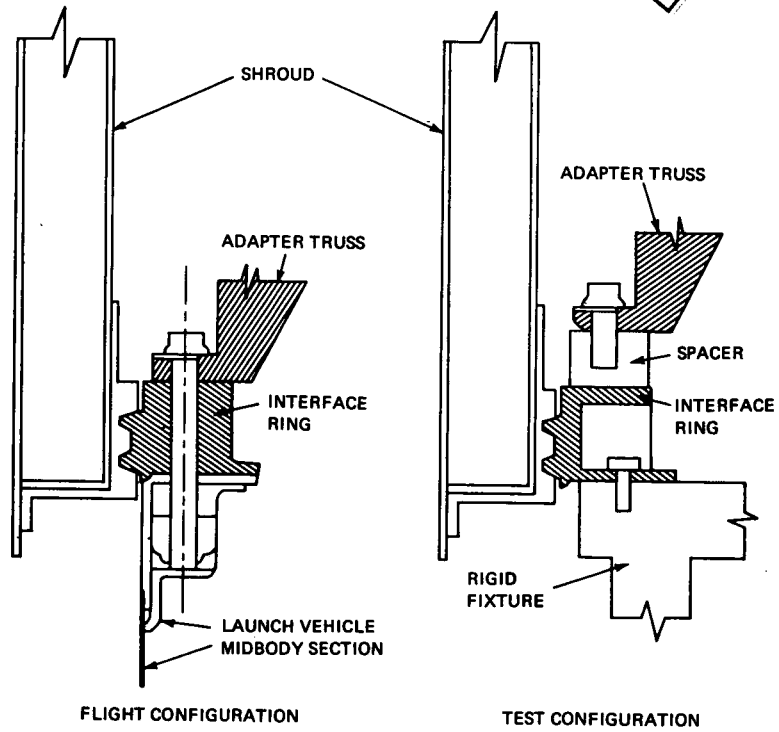TEST CONFIGURATION

Figure 3. Spacecraft/shroud Interface

4

frequency energy via the mechanical path would not be adversely affected by the use of a more rigid fixture, the tests were conducted with the readily available rigid fixture.

Acoustic Facility

The tests were accomplished utilizing the acoustic system installed on the LPS (Reference 1). A sketch of the LPS test chamber (Figure 4) illustrates the test setup for tests with the shroud installed (SI tests) and with the shroud removed (SR tests). The test fixture is used to position the shroud/spacecraft package to the optimum design location within the test chamber.

The SI tests had the acoustic liner in place, whereas the SR tests had the liner removed. The purpose of the liner is to provide a progressive wave field that is contained within the liner and is external to the spacecraft shroud, much like the actual flight environment. When the liner is removed, the LPS functions as a semireverberant chamber that to some extent duplicates the true environmental condition that would have been present within the shroud.

The acoustic input is generated by a noise generator/acoustic horn system capable of overall levels of 155 dB and with a continuous spectrum of 100 to 12 000 Hz.

Instrumentation

A total of 35 accelerometers mounted at 16 different model locations were used to monitor the model's dynamic response. Table 1, together with Figure 5, presents a detailed tabulation of the accelerometer designations and complete description of their exact locations. The accelerometer locations can be broken down into four general groups:

(1) Those on the spacecraft adapter truss (16 total, six locations).

(2) Those on the solar array and EP-6 boom (five total, two locations).

(3) Those on the spacecraft experiment panels within the spacecraft box (11 total, seven locations).

(4) Those on top of the spacecraft box (three total, one location).

An attempt was made in selecting the mounting locations to see if there were differences among the responses monitored from primary structural members (group 1), from various spacecraft appendages (group 2), and from the basic structure that supports and encloses the spacecraft experiments (groups 3 and 4).

Fifteen microphones were installed to record the acoustic excitation both exterior to the shroud and within the shroud as well. Figures 6 and 7 illustrate their mounting locations.

During each test, the microphone and accelerometer responses were recorded on magnetic tape for future analysis. In addition, selected channels were also displayed on an oscillograph to provide quick-look analysis and to ensure that clipped data were avoided.
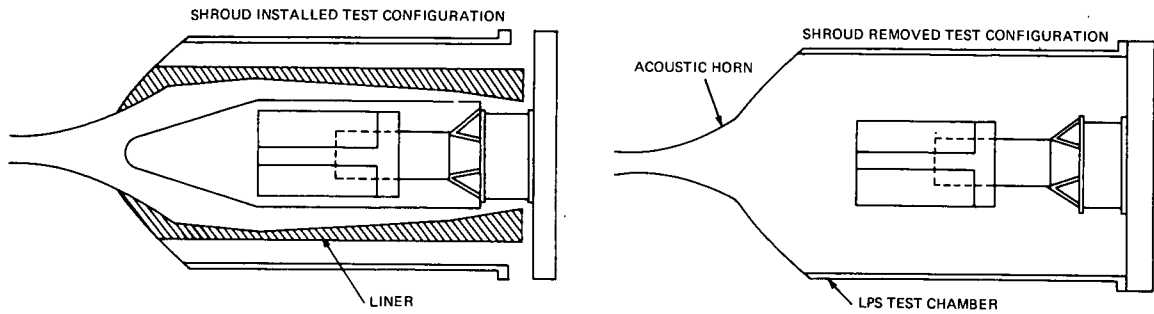
SHROUD INSTALLED TEST CONFIGURATION

SHROUD REMOVED TEST CONFIGURATION

ACOUSTIC HORN

LINER

LPS TEST CHAMBER

Figure 4. Test Configurations

TABLE 1
ACCELEROMETER LOCATIONS

Location	Accelerometer*	Description of Location
1	1X, 1Y, 1Z	base of spacecraft adapter truss (−X, +Z corner)
2	2X, 2Y, 2Z	base of spacecraft adapter truss (+X, +Z corner)
3	3X, 3Y, 3Z	top of spacecraft adapter truss (−X, +Z corner)
4	4X, 4Y, 4Z	top of spacecraft adapter truss (+X, +Z corner)
5	5X, 5Y, 5Z	top of spacecraft (+X, −Z corner)
6	6X, 6Z	+X solar array (half way between supports)
7	7X, 7Y, 7Z	top of folded EP-6 boom
8	8X, 8Y, 8Z	+Z experiment panel (station 337)
9	9X, 9Y, 9Z	−X panel (near battery unit 2)
10	10Z	+Z experiment panel (station 362)
11	11Z	−Z experiment panel (station 364)
12	12Z	−Z experiment panel (station 337)
13	13Z	−Z experiment panel
14	14X	−Z side of intercostal panel
15	15X	end cap (adjacent to +X, +Z adapter truss leg)
16	16X, 16Y, 16Z	end cap (adjacent to −X, +Z adapter truss leg)

*X, Y, and Z denote axes of measurement.
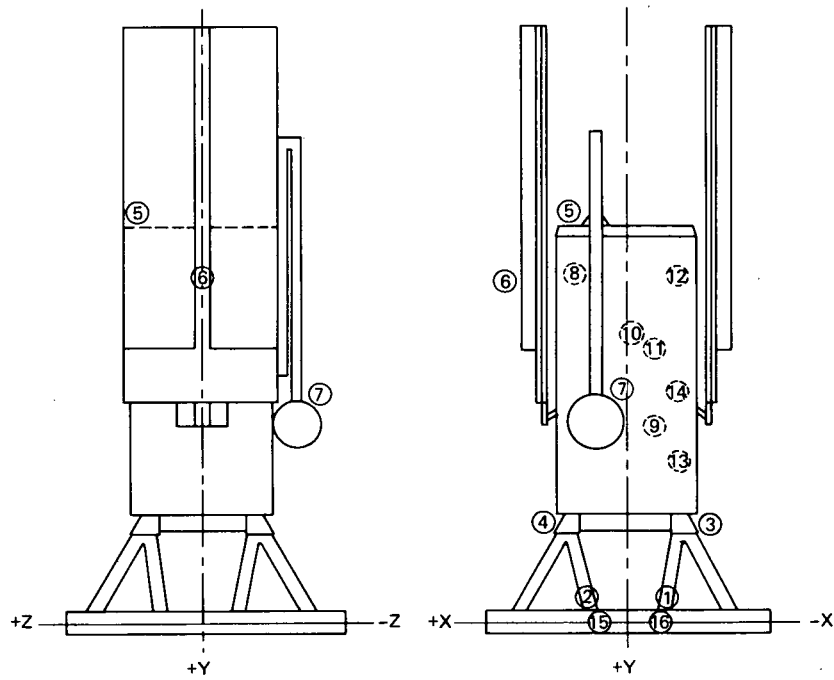
LOCATIONS 1 THROUGH 7 ARE EXTERNAL LOCATIONS.
LOCATIONS 8 THROUGH 14 ARE WITHIN THE SPACECRAFT BOX.
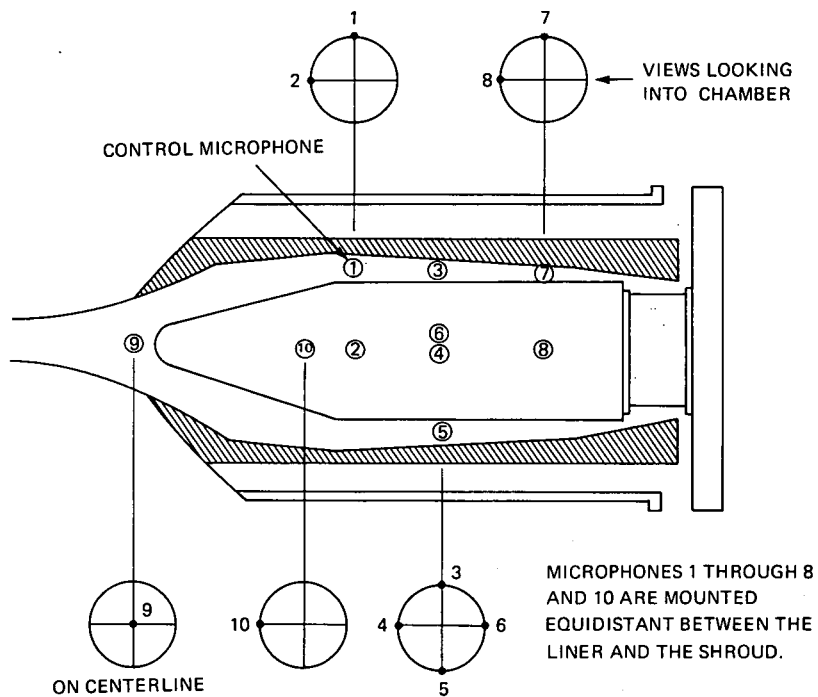
Figure 5. Accelerometer Locations

CONTROL MICROPHONE

VIEWS LOOKING
INTO CHAMBER

MICROPHONES 1 THROUGH 8
AND 10 ARE MOUNTED
EQUIDISTANT BETWEEN THE
LINER AND THE SHROUD.

ON CENTERLINE

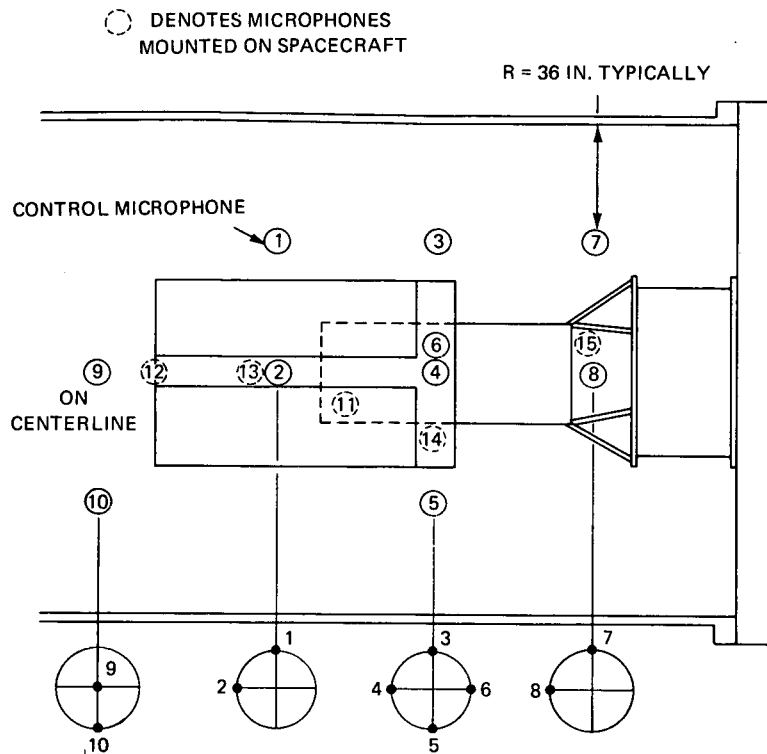Figure 6. SI Test: External Microphone Locations

Figure 7. SR Test: Microphone Locations

TEST PROCEDURE AND PHILOSOPHY

For the SI tests, the acoustic input exterior to the shroud was controlled to match the Atlas-Agena flight acoustic spectrum test specification. For the SR tests, the internal levels measured during the SI tests were used as the basis of control. The test philosophy adhered to throughout the tests was to attempt to maintain the identical acoustic input spectrum acting directly on the spacecraft in order to evaluate the effects of shroud removal. Stated more simply, the SR tests were specified to be equivalent to the SI tests as far as acoustic noise input to the spacecraft was concerned.

TEST RESULTS

Microphone Analysis

A one-third octave band level analysis was performed for each microphone channel. Figure 8 presents the average sound pressure level (SPL) (in decibels) versus the one-third octave band center frequency for both the SI and SR tests.

8

Figure 9 presents P versus center frequency, where

$$P_i = p_i^2 / \Sigma p_i^2 \ ,$$

in which Σp_i^2 is the mean-square pressure. The parameter P indicates that portion of the overall p mean-square level contributed by each particular one-third octave band.

From the external and internal SPL plots, a plot of the noise reduction (in decibels) of the shroud was obtained (Figure 10). The dip in the shroud noise reduction curve at 630 Hz is to be expected since a minimum in the noise reduction of a cylindrical shroud will be found at the shroud ring frequency (Reference 2). For the shroud parameters used,

$$f_{\text{ring}} = \frac{C}{2\pi r}$$

$$= 590 \text{ Hz} \ ,$$

where r is the radius of the shroud, 0.82 m (2.7 ft), and c is the longitudinal wavespeed through the shroud material, 3048 m/s (10 000 ft/s).

Accelerometer Analysis

Power spectral density (PSD) digital plots (in g^2/Hz versus frequency) were obtained from all accelerometer channels (49 total). PSD plots from selected representative channels are given in Figures 11 through 15 for the SI tests and Figures 16 through 20 for the SR tests. The recorded accelerometer responses were converted by an analog-to-digital system to a digital format on a magnetic tape. This tape was then processed by the Dyvan Computer Program (Reference 3), which generates a plot tape containing the desired information. An electronic plotter reads the plot tape and produces the final hard-copy plots. The use of the digital approach reduces the PSD reduction task by a factor of 15 (4 hours to produce a digital tape and 5 seconds per electronic plot as compared with about 60 hours for analog analysis).

The accelerometer g_{rms}-levels for the SR and SI tests are tabulated in Table 2. In addition, normalized g_{rms}-levels, where the accelerometer response is normalized to the SI test accelerometer values, are given.

A one-third octave band level analysis was also performed for each accelerometer response and converted to a decibel scale normalized to a $1 g_{\text{rms}}$ reference (as illustrated in Figure 21).
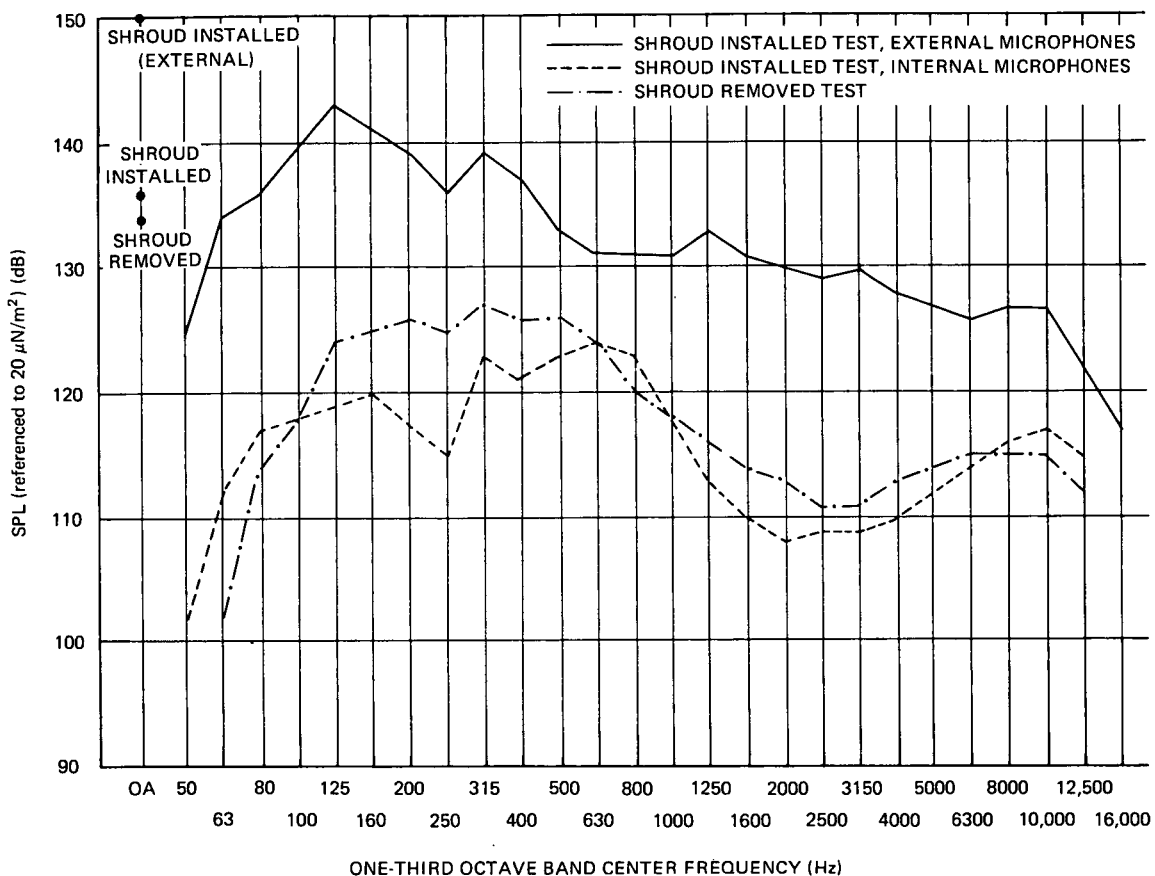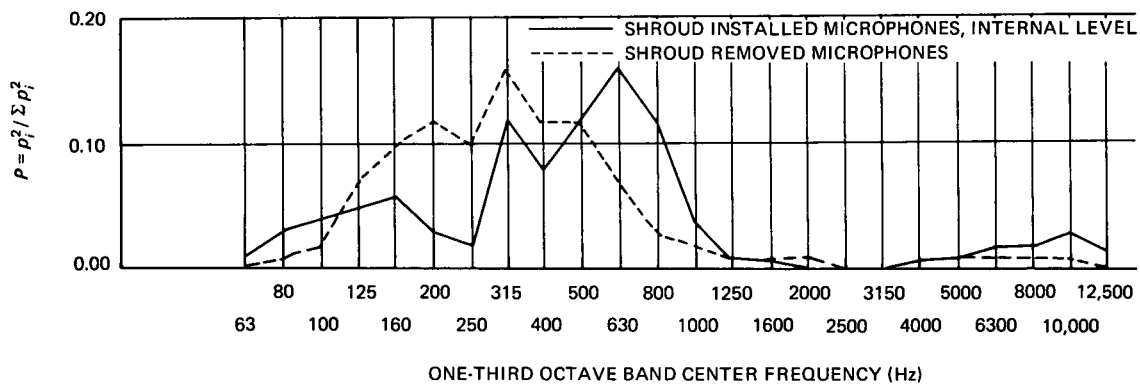
9

Figure 8. SI and SR Sound Pressure Levels

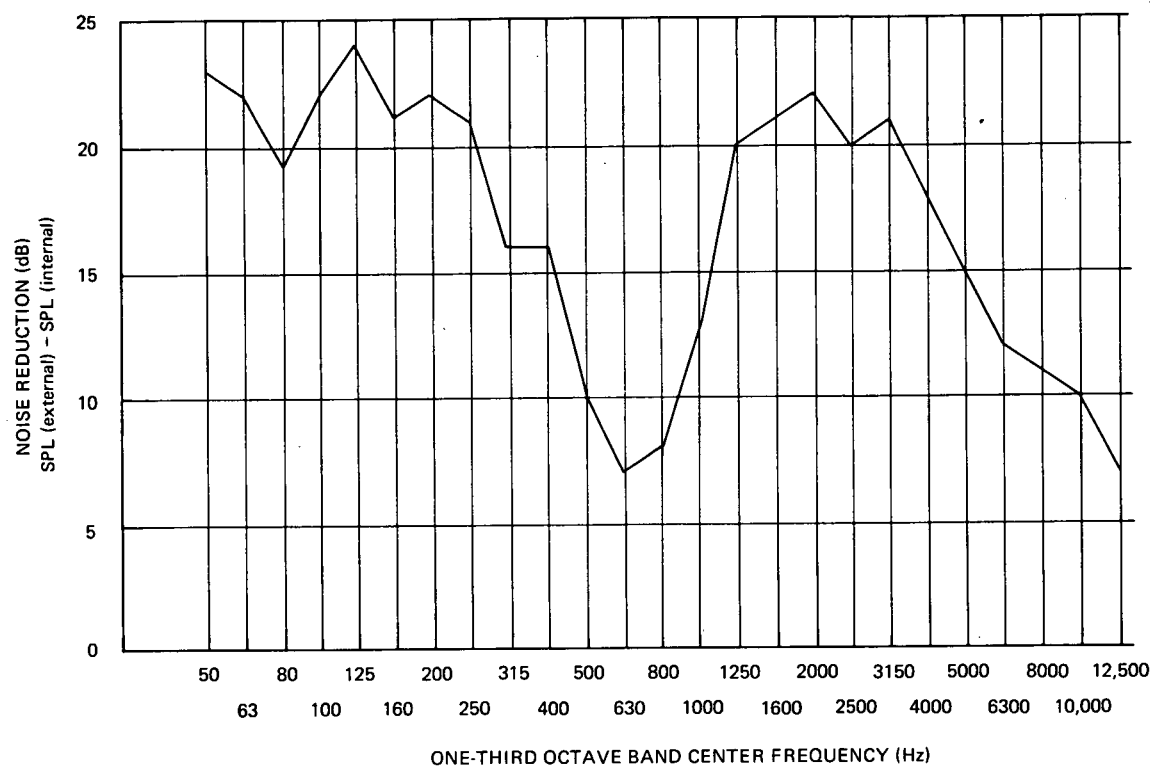
Figure 9. *P* versus Center Frequency

10

Figure 10. Shroud Noise Reduction

11

PSD DIGITAL PLOT

1.63 g_{rms}

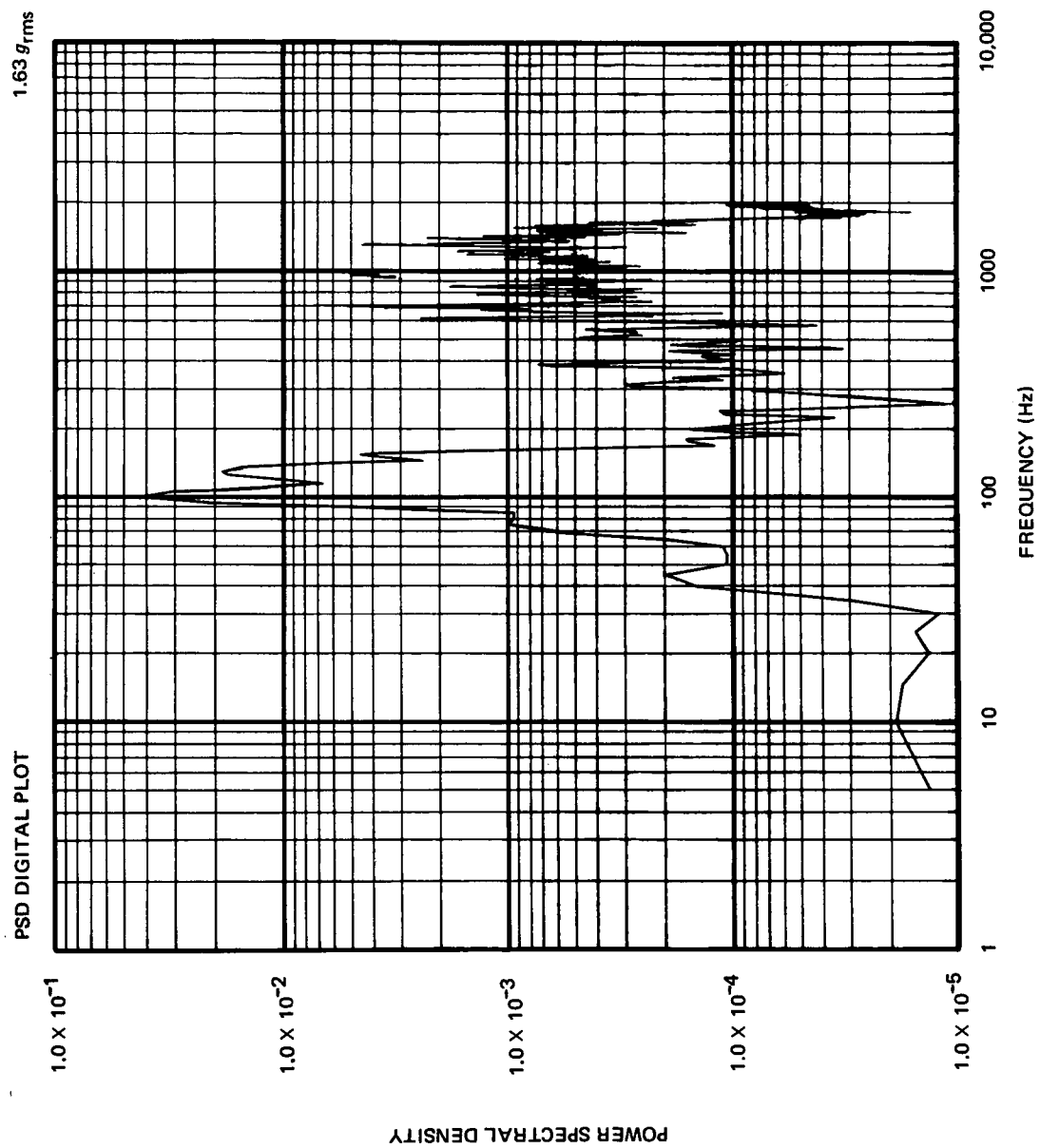Figure 11. Accelerometer Response in Shroud-installed Test
at Location 2Z, Base of Spacecraft Adapter Truss

FREQUENCY (Hz)

POWER SPECTRAL DENSITY

12

PSD DIGITAL PLOT

0.99 g_{rms}
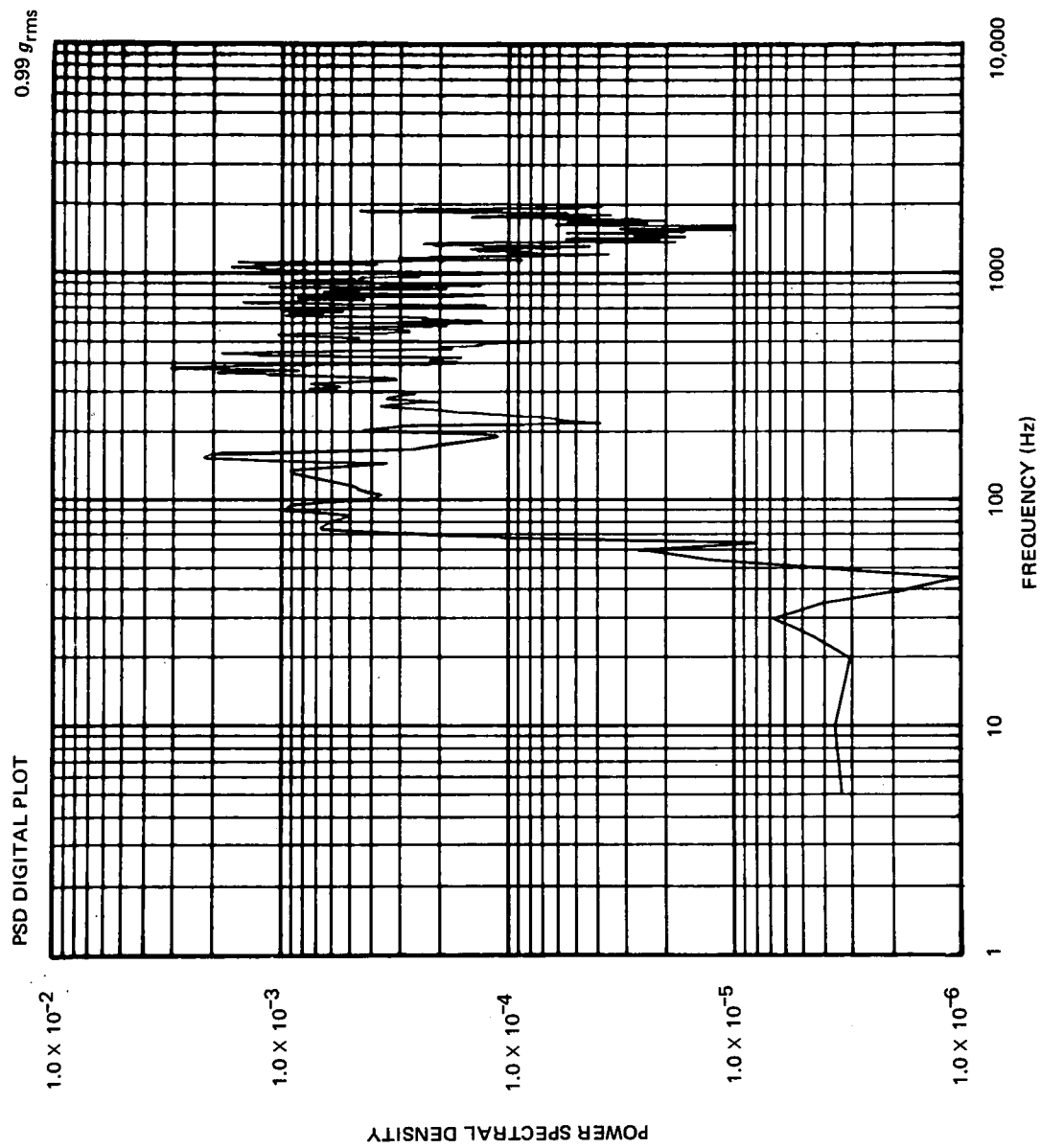
Figure 12. Accelerometer Response in Shroud-installed Test
at Location 4X, Top of Spacecraft Adapter Truss

13

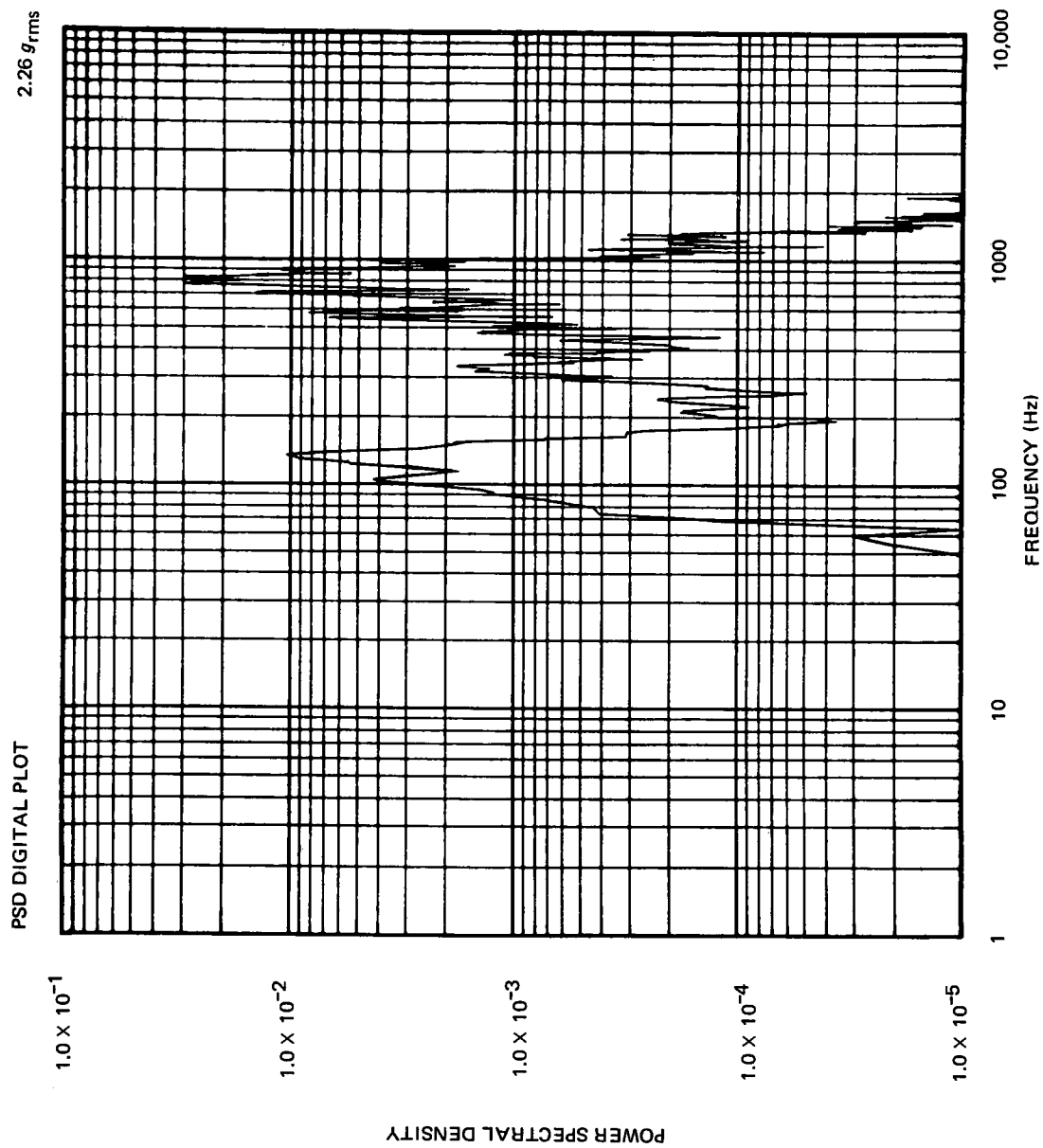PSD DIGITAL PLOT   2.26 g_{rms}
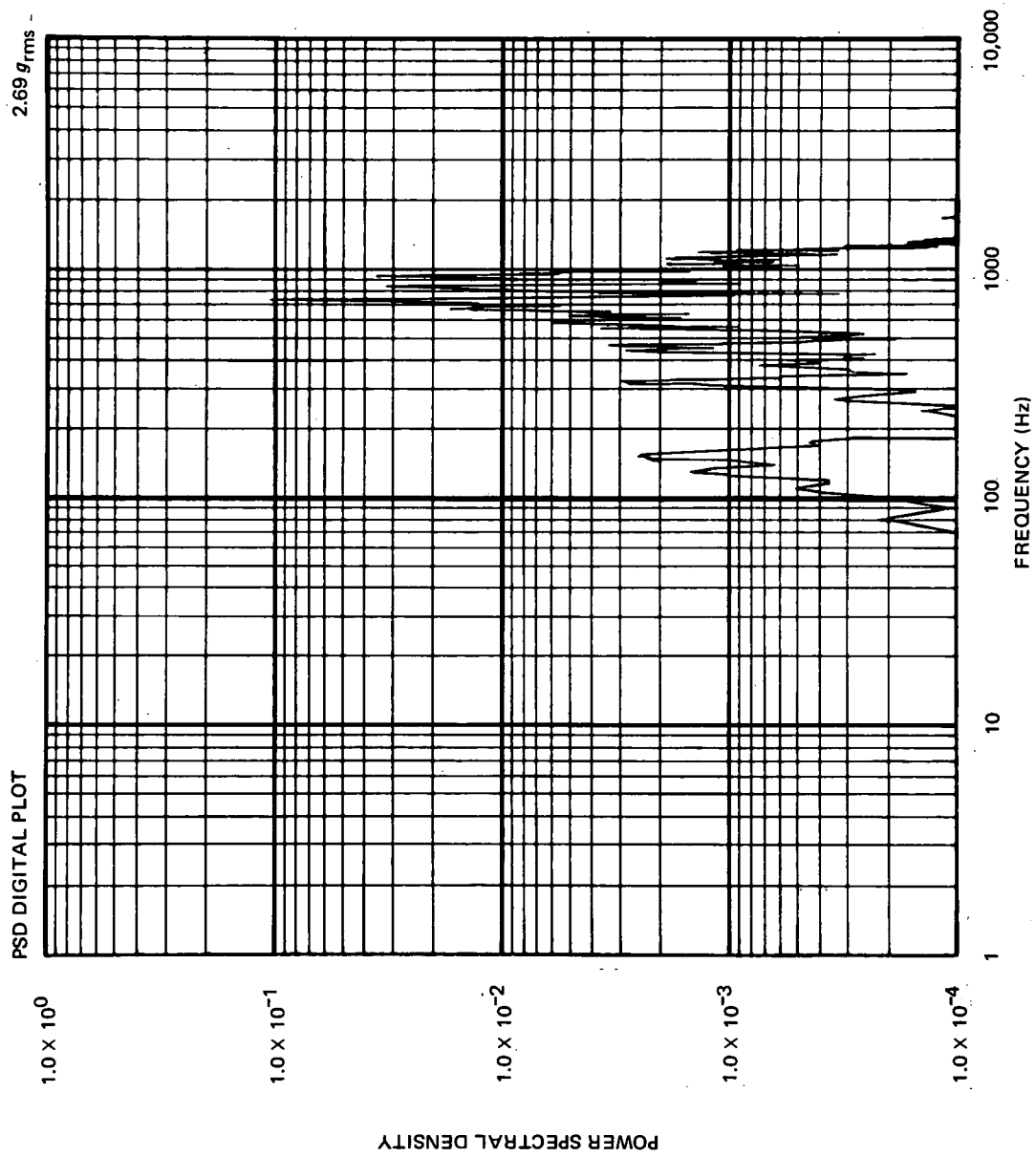

Figure 13. Accelerometer Response in Shroud-installed Test
at Location 5Y, Top of Spacecraft

14

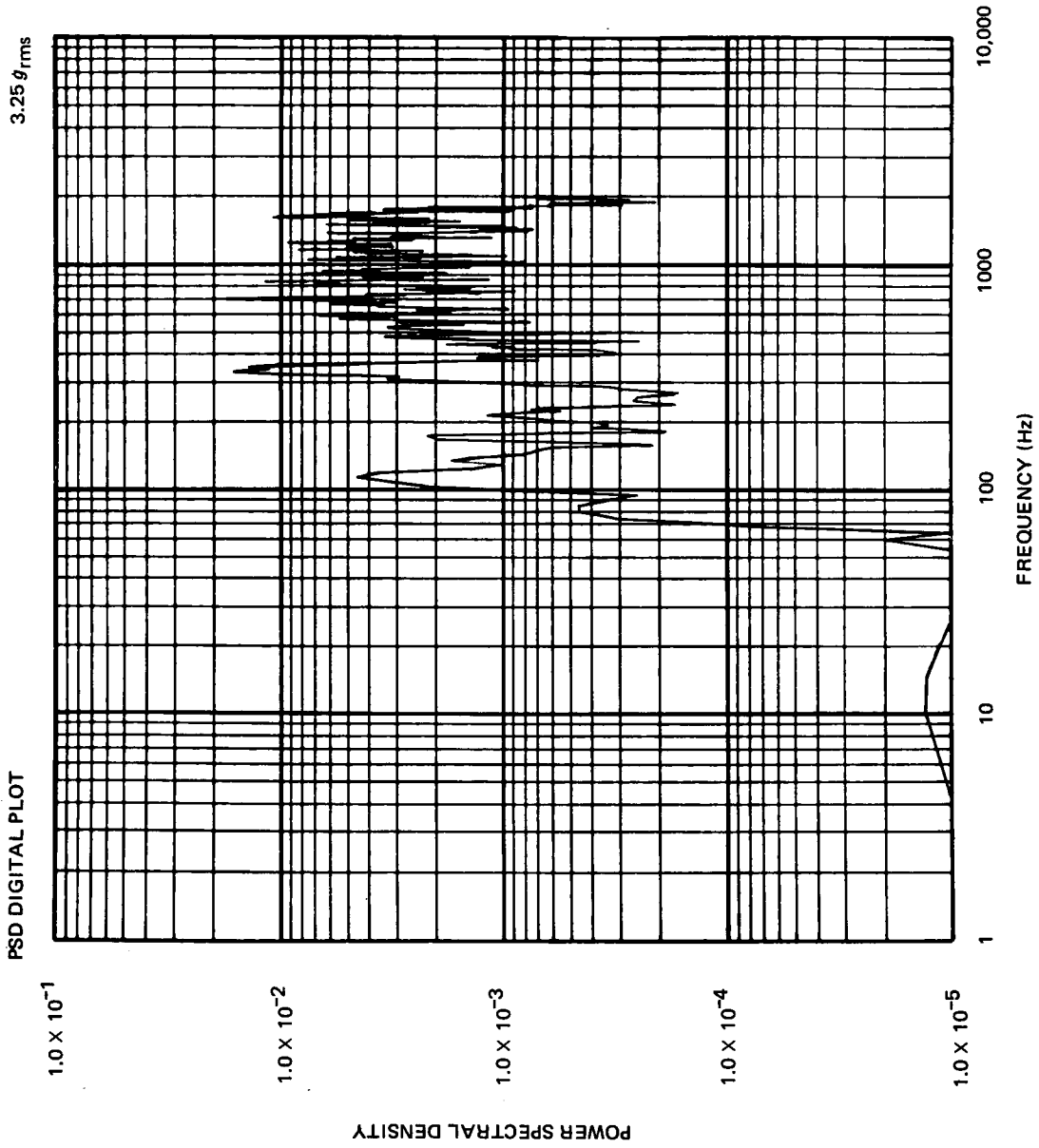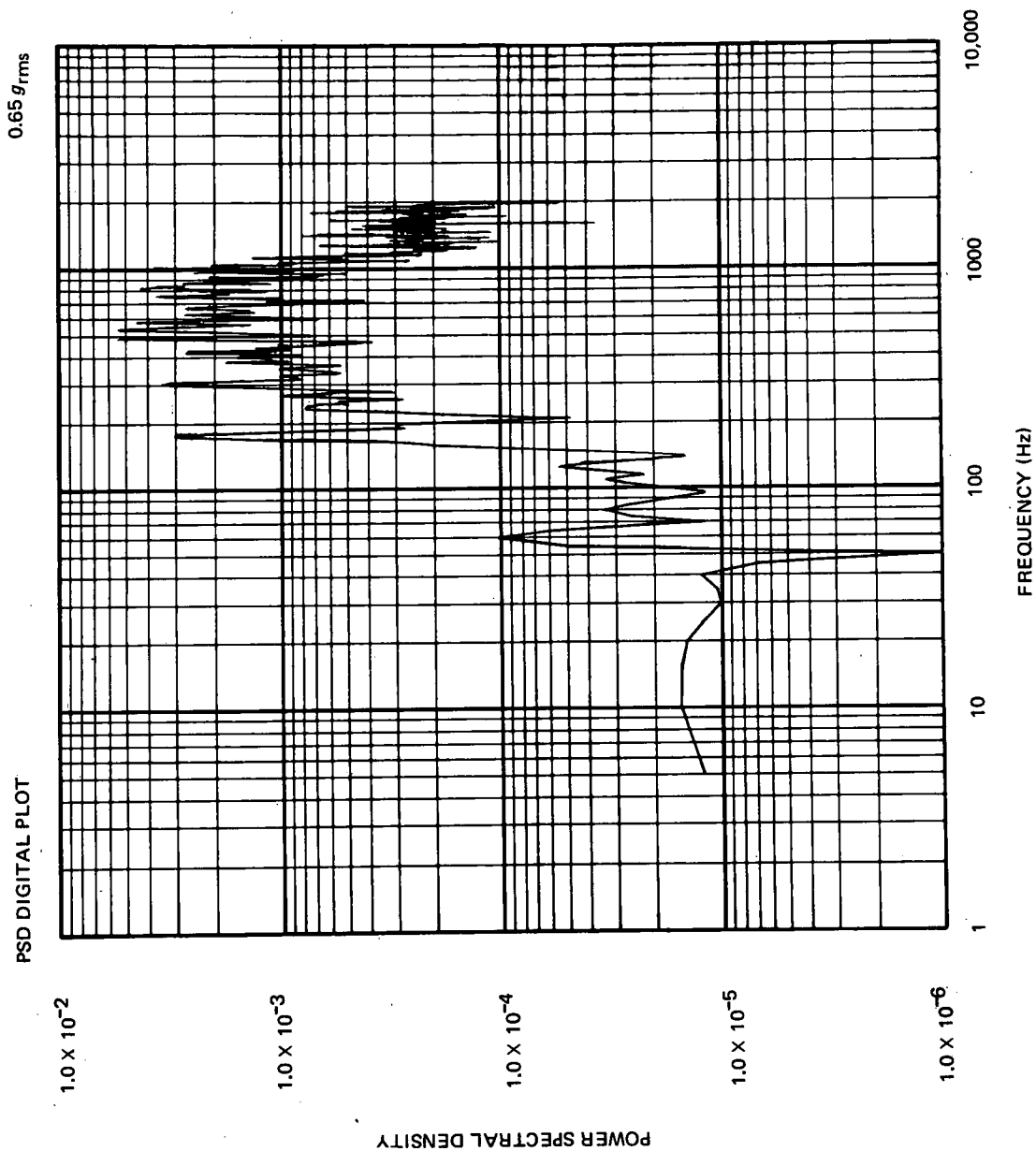Figure 14. Accelerometer Response in Shroud-installed Test at Location 6X on Solar Array

15

PSD DIGITAL PLOT

3.25 g_{rms}

POWER SPECTRAL DENSITY

FREQUENCY (Hz)

Figure 15. Accelerometer Response in Shroud-installed Test at Location 8Z, +Z Experiment Panel

16

PSD DIGITAL PLOT

0.65 g_{rms}

POWER SPECTRAL DENSITY

1.0 × 10^{-2}

1.0 × 10^{-3}

1.0 × 10^{-4}

1.0 × 10^{-5}

1.0 × 10^{-6}

1   10   100   1000   10,000

FREQUENCY (Hz)

Figure 16. Accelerometer Response in Shroud-removed Test
at Location 2Z, Base of Spacecraft Adapter Truss

17

PSD DIGITAL PLOT

0.78 g_{rms}

POWER SPECTRAL DENSITY

1.0 X 10^{-3} 1.0 X 10^{-4} 1.0 X 10^{-5} 1.0 X 10^{-6} 1.0 X 10^{-7}

FREQUENCY (Hz)

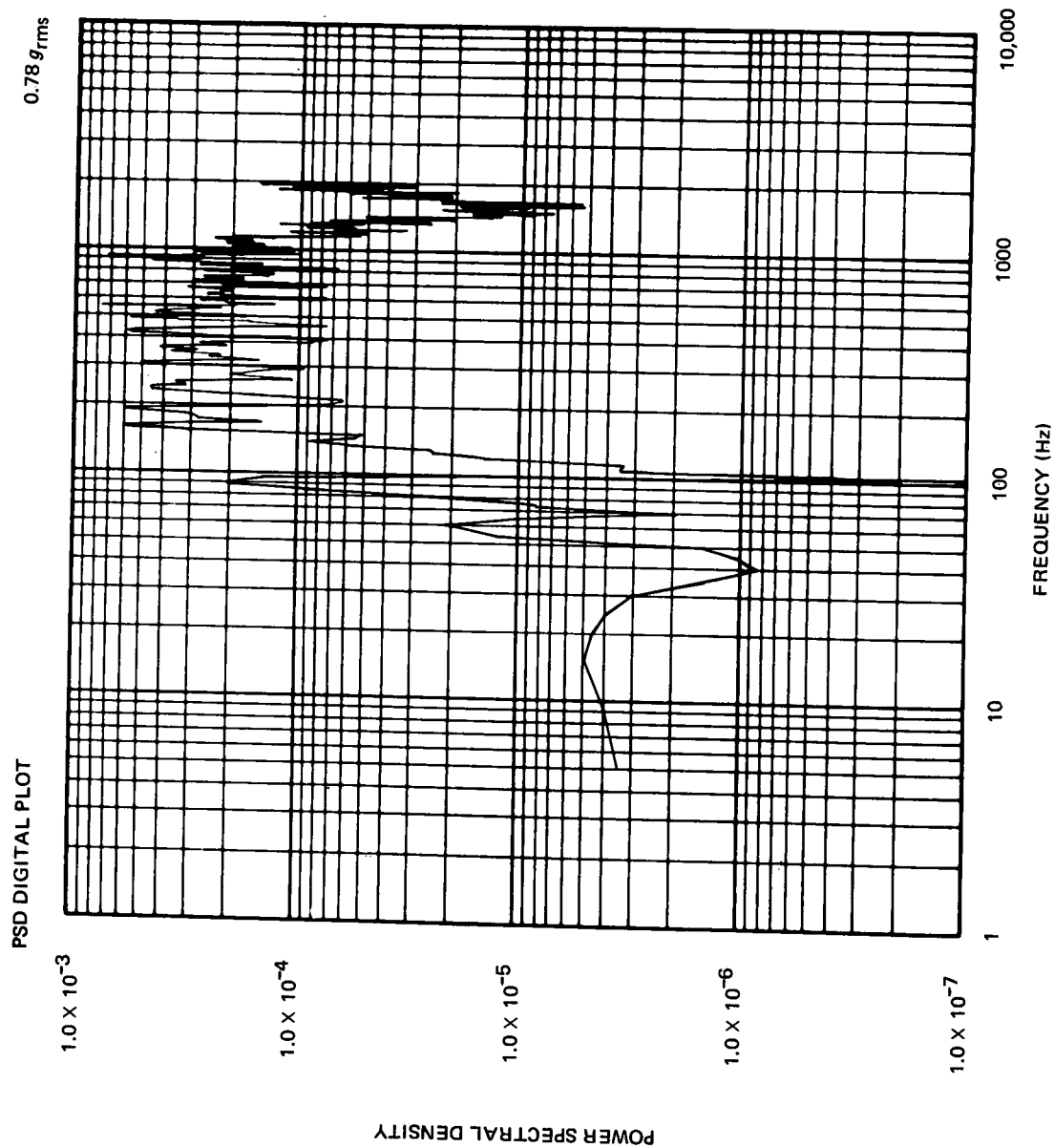1   10   100   1000   10,000

Figure 17. Accelerometer Response in Shroud-removed Test
at Location 4X, Top of Spacecraft Adapter Truss

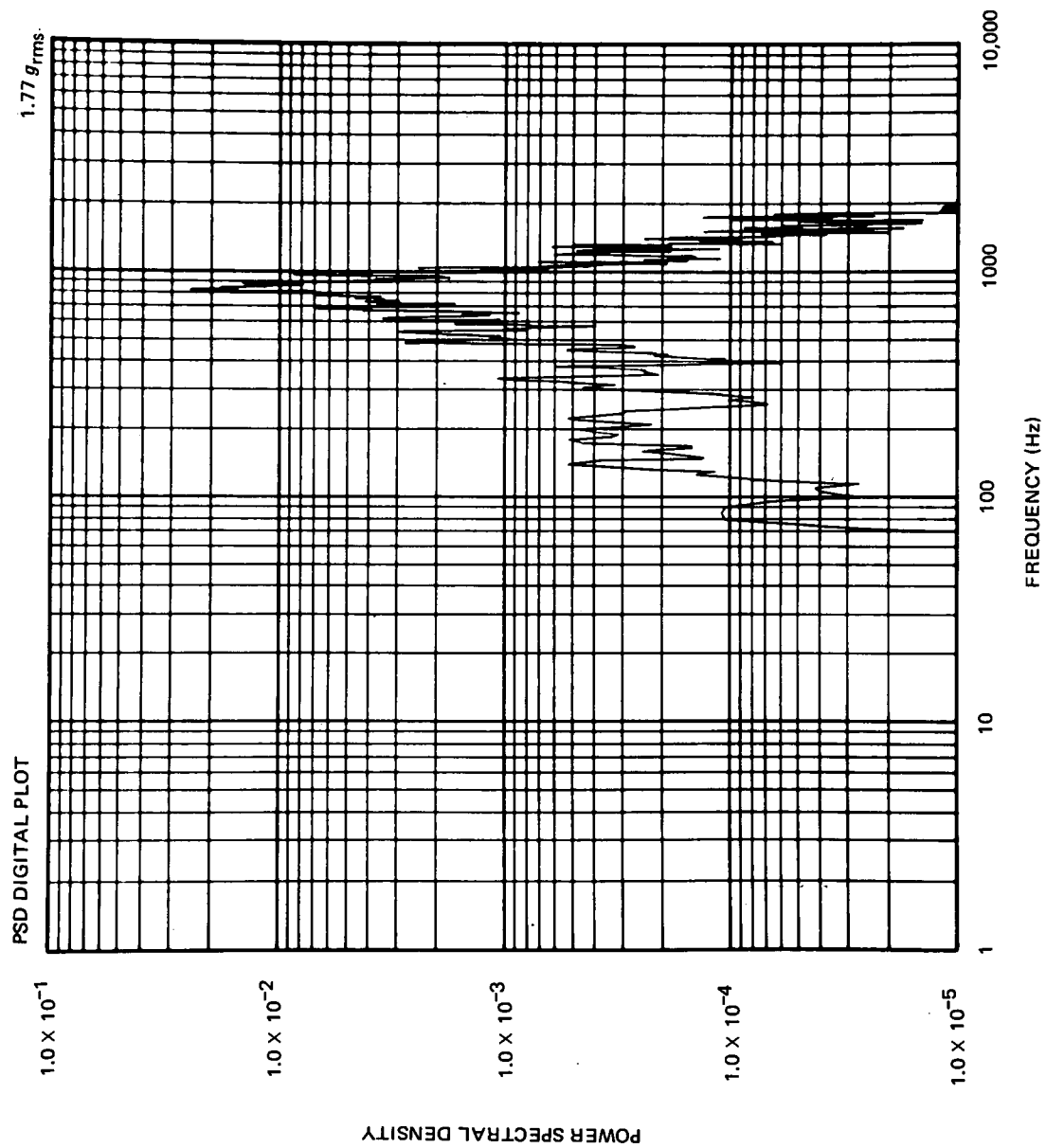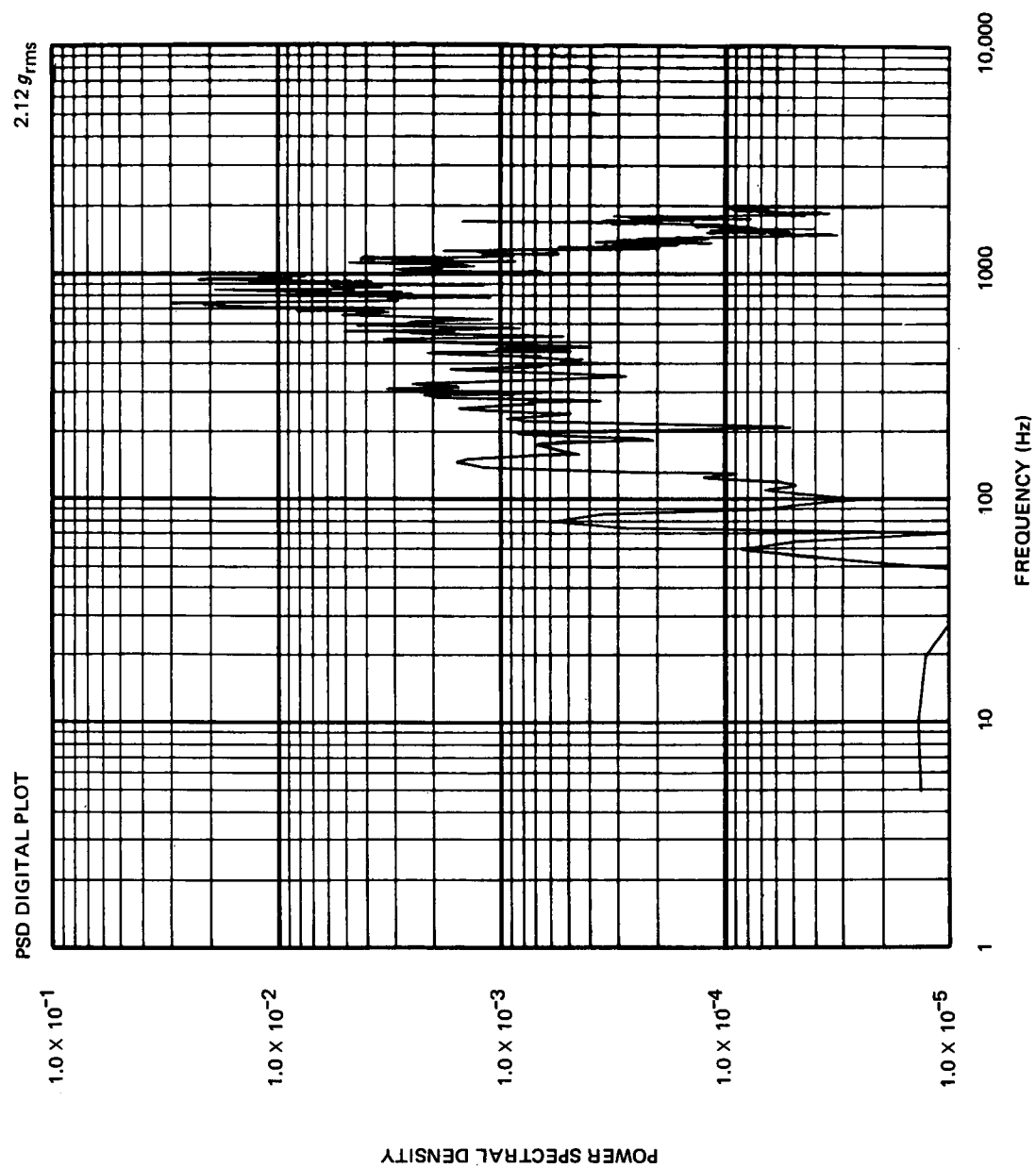Figure 18. Accelerometer Response in Shroud-removed Test at Location 5Y, Top of Spacecraft

19

PSD DIGITAL PLOT

2.12 g_{rms}

POWER SPECTRAL DENSITY

1.0 X 10^{-1}

1.0 X 10^{-2}

1.0 X 10^{-3}

1.0 X 10^{-4}

1.0 X 10^{-5}

1   10   100   1000   10,000

FREQUENCY (Hz)

Figure 19. Accelerometer Response in Shroud-removed Test
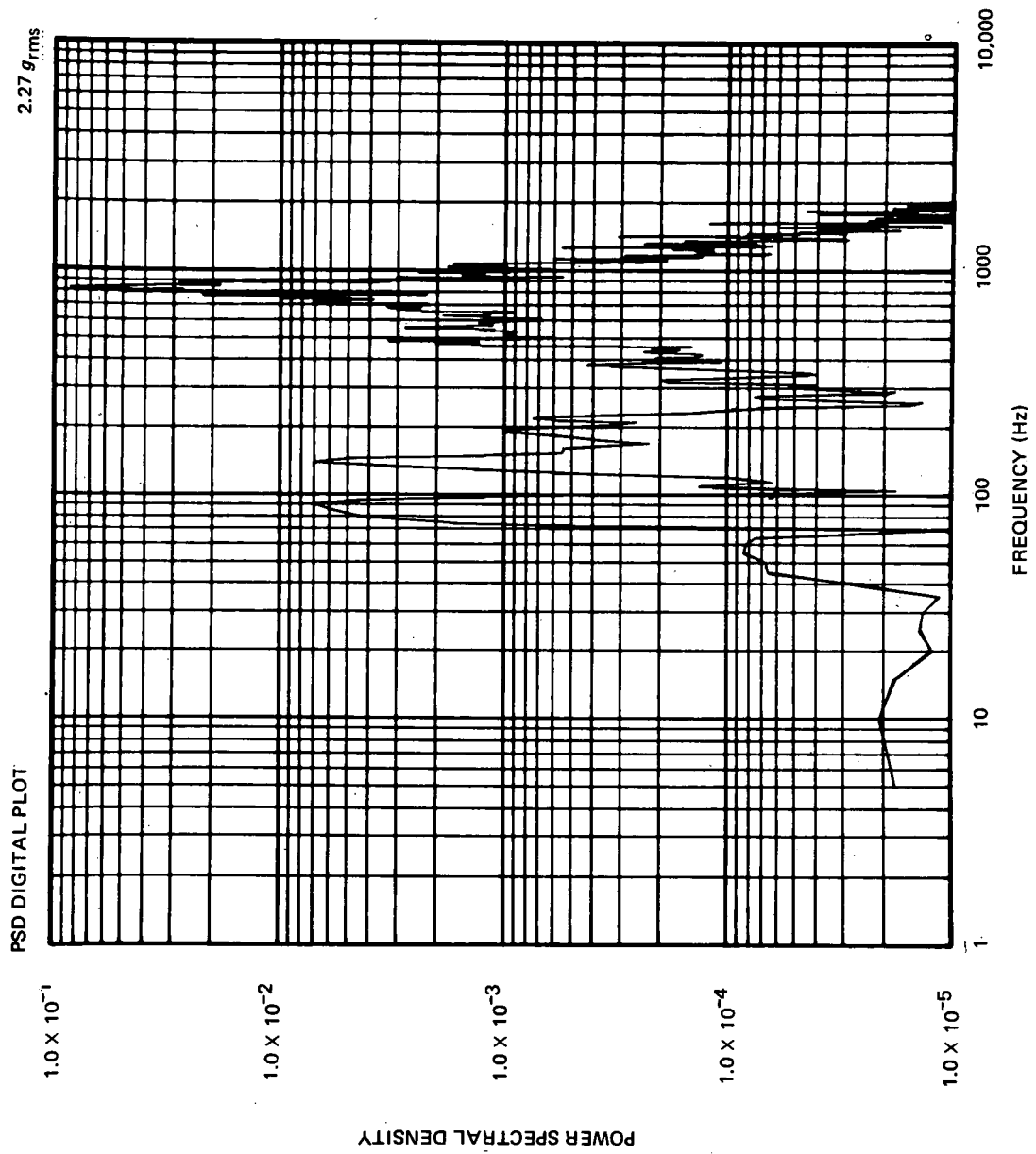at Location 6X on Solar Array

20

Figure 20. Accelerometer Response in Shroud-removed Test at Location 8Z, +Z Experiment Panel

21

TABLE 2
ACCELEROMETER RESPONSE

| Location	Accelerometer	SI Test (g_{rms})	SR Test (g_{rms})	SR/SI
Base of adapter truss	1X	1.63	0.95	0.58
	1Y	2.26	0.66	0.29
	1Z	—	1.16	—
	2X	—	0.89	—
	2Y	—	0.65	—
	2Z	1.63	1.05	0.64
Top of adapter truss	3X	3.18	0.82	0.26
	3Y	1.34	0.63	0.47
	3Z	0.78	0.61	0.78
	4X	0.99	0.78	0.79
	4Y	1.13	0.54	0.48
	4Z	0.88	0.59	0.67
Top of spacecraft	5X	1.51	1.41	0.93
	5Y	2.26	1.77	0.78
	5Z	2.33	2.12	0.91
Solar array	6X	2.69	2.12	0.79
	6Z	1.24	1.48	1.19
EP-6 boom	7X	1.10	1.34	1.22
	7Y	1.13	1.06	0.94
	7Z	1.16	1.22	1.05
Experiment panels	8X	—	1.52	—
	8Y	3.39	2.12	0.63
	8Z	3.25	2.27	0.70
	9X	—	0.44	—
	9Y	—	0.82	—
	9Z	—	0.51	—
	10Z	2.69	1.70	0.63
	11Z	0.99	2.76	2.79
	12Z	1.63	1.77	1.09
	13Z	3.71	3.32	0.89
	14X	0.72	0.35	0.49
End cap near truss	15Y	—	0.21	—
	16X	—	0.13	—
	16Y	—	0.21	—
	16Z	—	0.11	—
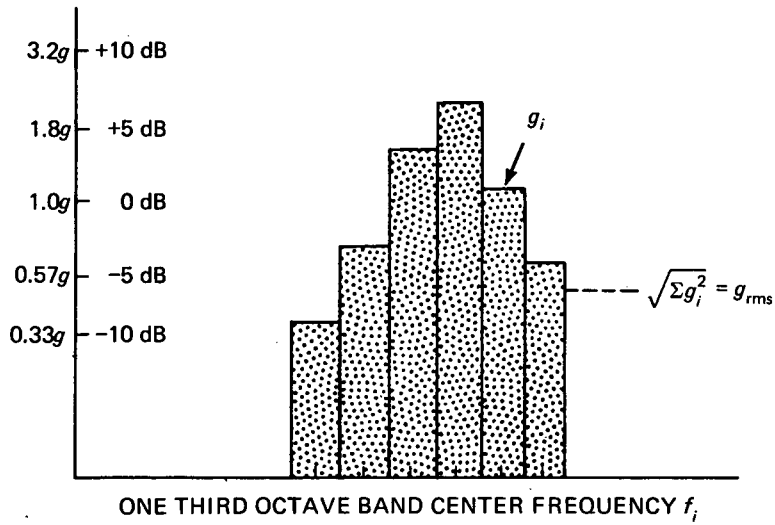
Figure 21. Accelerometer One-third Octave Band Level Analysis

The acceleration level (AL) of an individual accelerometer is defined by

$$AL \text{ (dB)} = 10 \log_{10} \frac{g_i^2}{g_0^2} \; ,$$

where

g_i = rms acceleration at a particular center frequency

g_0 = $1 g_{rms}$ reference.

Additionally, one can also determine the quantity G, where

$$G_i = g_i^2 / \Sigma g_i^2 \; ,$$

in which Σg_i^2 is the mean-square acceleration. The parameter G indicates that portion (in percent) of the overall g mean-square level contributed by each particular one-third octave band. Plots of G versus one-third octave band center frequency are given in Figures 22 through 27.

Combined Analysis

As a means of comparing the results of the SI tests with those of the SR tests, the accelerometer responses were normalized to a unit acoustic level input. This normalization was done by dividing the accelerometer responses by an averaged acoustic pressure. When
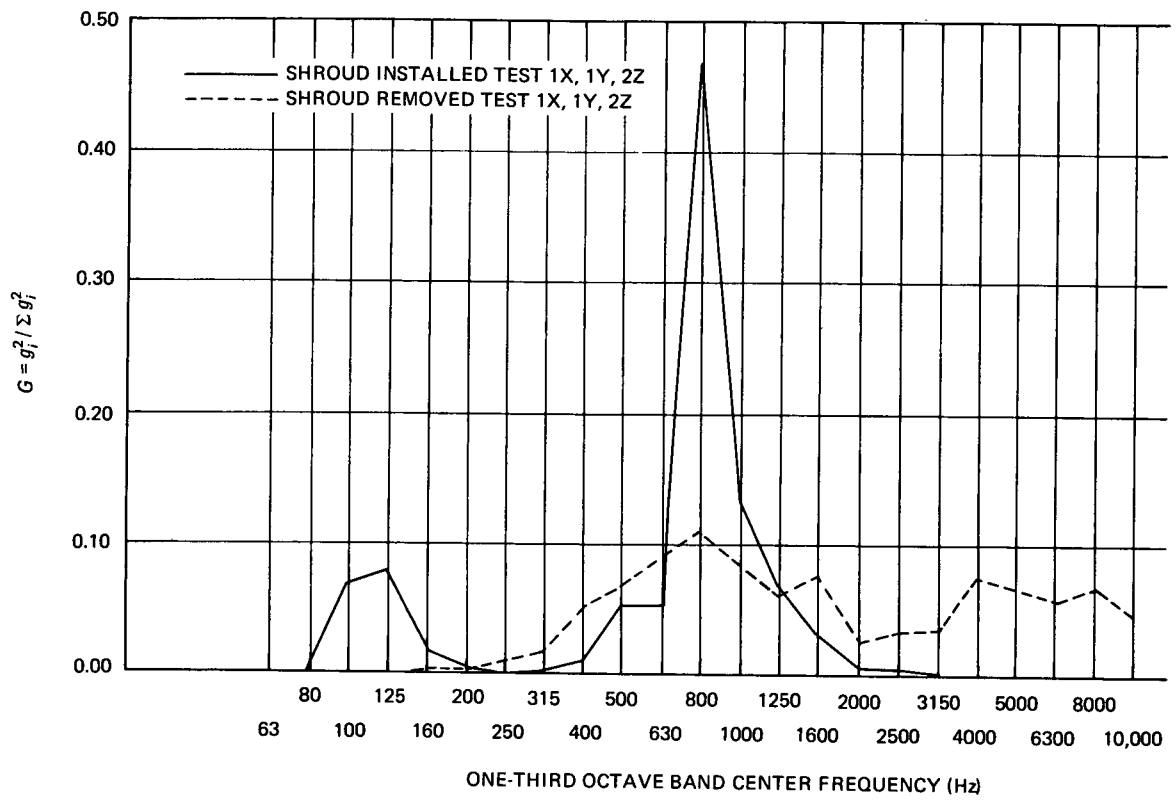
Figure 22. *G* versus Center Frequency, Base of Truss

the quantities involved are expressed in decibel form, this operation is defined by

$$SPL = 10 \log \frac{\bar{p}_i^2}{p_0^2} \quad ,$$

where

$\bar{p}_i$ = average microphone level

$p_0 = 20 \ \mu N/m^2 \ (0.0002 \ \mu b)$,

$$AL = 10 \log \frac{g_i^2}{g_0^2} \quad ,$$

where

g_i = individual accelerometer response

$g_0 = 1 g_{rms}$.
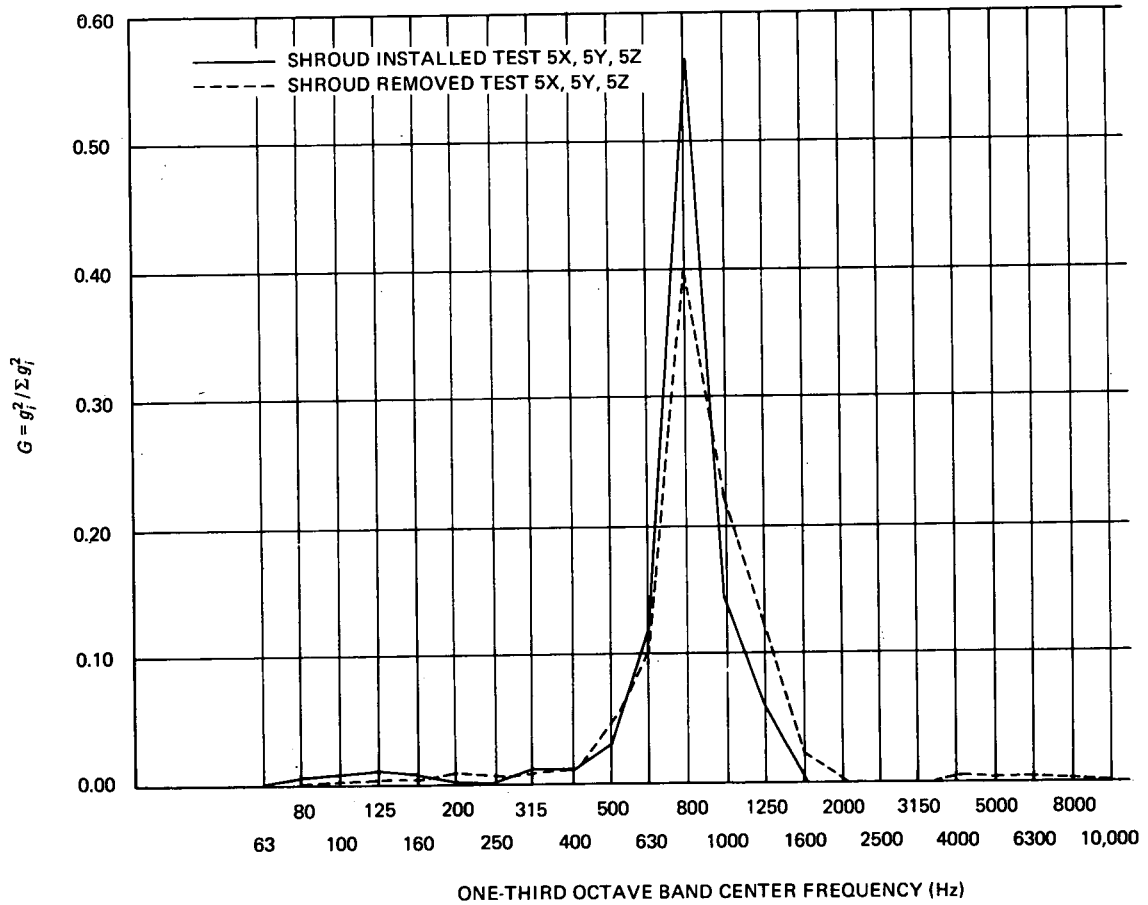
24
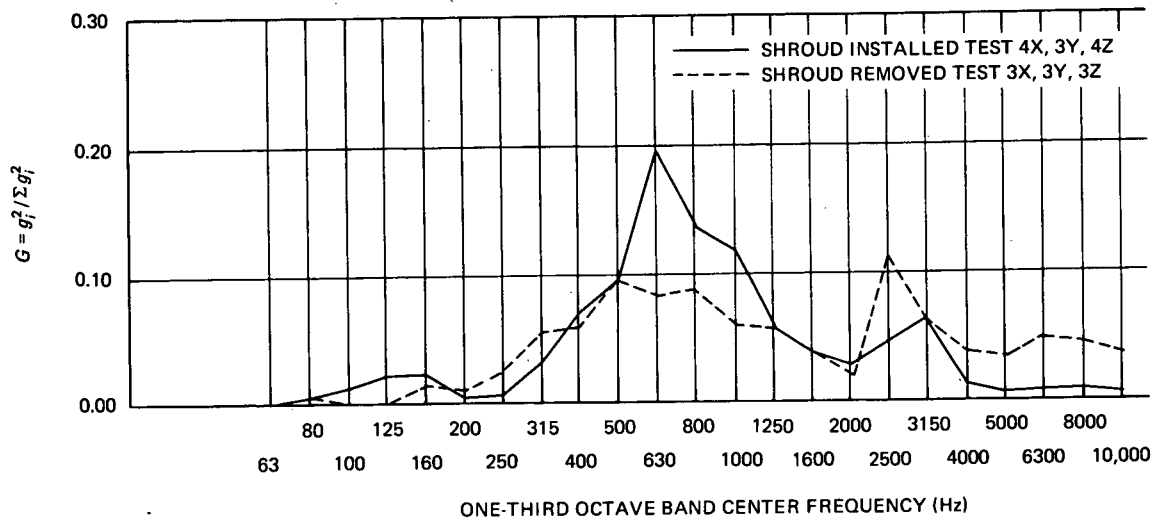
Figure 23. *G* versus Center Frequency, Top of Truss

Figure 24. *G* versus Center Frequency, Top of Spacecraft

25
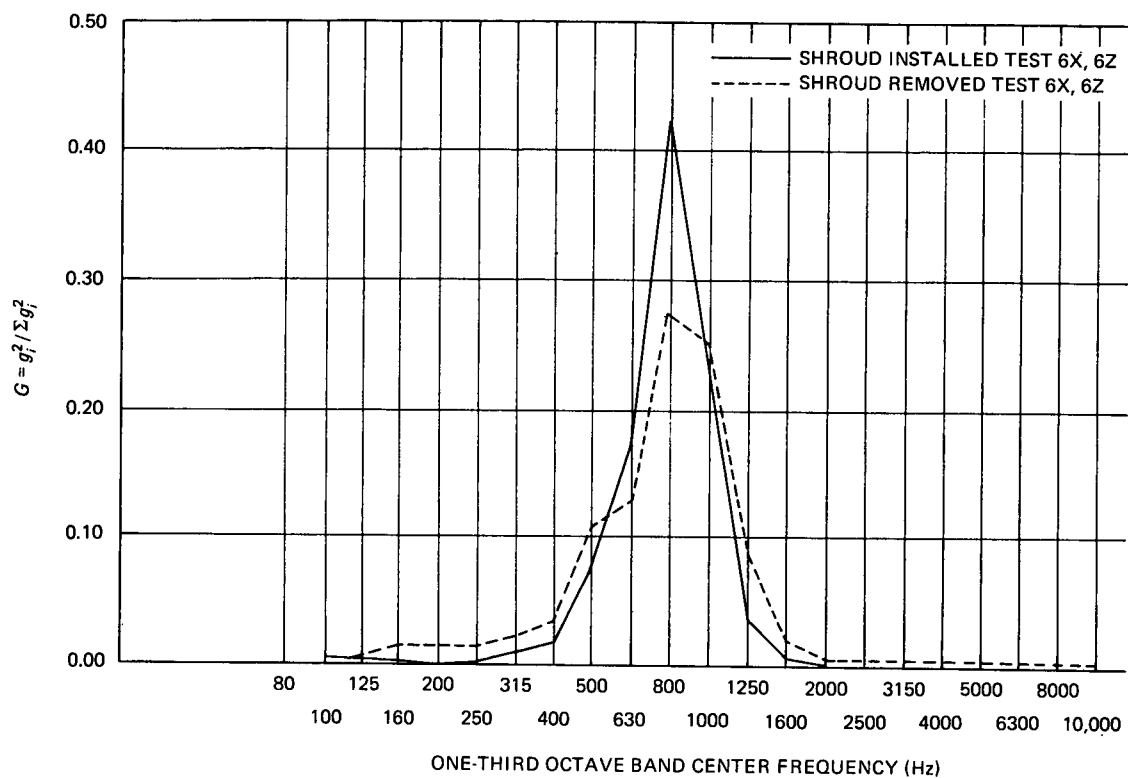
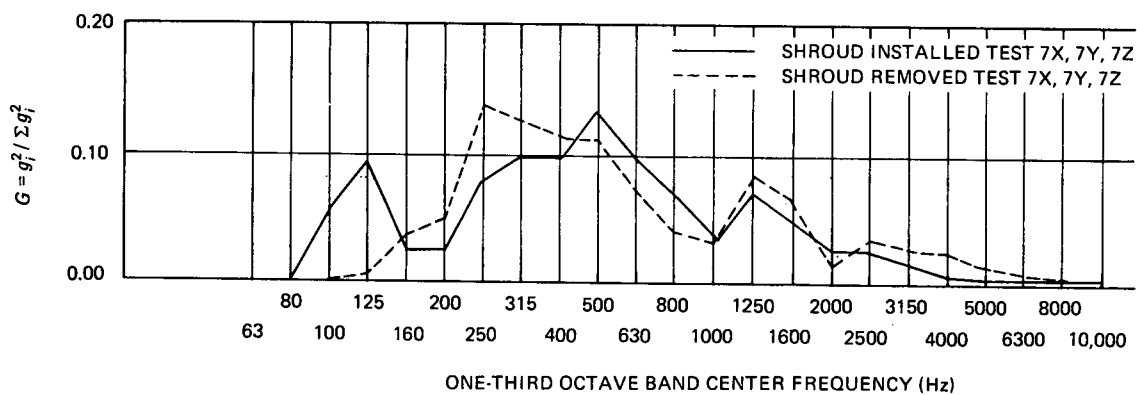Figure 25. *G* versus Center Frequency, Solar Array

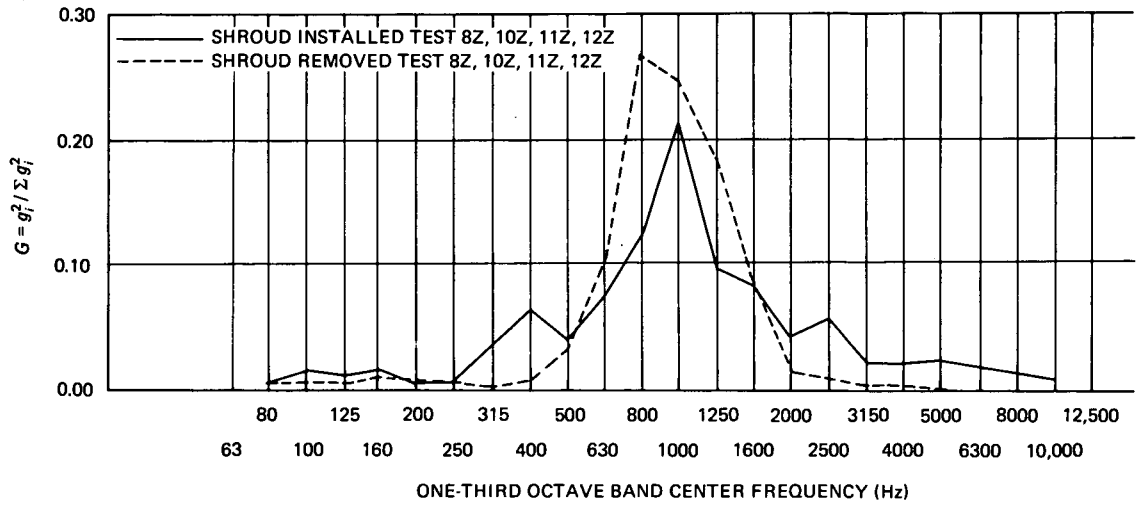Figure 26. *G* versus Center Frequency, Top of Folded EP-6 Boom

26

Figure 27. *G* versus Center Frequency, Experiment Panels

Then,

$$AL - SPL = 10 \log \frac{g_i^2/g_0^2}{\bar{p}_i^2/p_0^2} \ .$$

The quantity AL − SPL is evaluated for each one-third octave band center frequency.

The SPL microphone value used in the ratio represents the average value obtained from the internal microphone responses, also on a one-third octave basis. Figures 28 through 33 (SI tests) and Figures 34 through 39 (SR tests) present the individual accelerometer AL − SPL plots. In Figures 40 through 45, the individual plots are averaged to obtain the final comparisons of the SI and SR tests.

COMPARISON OF RESULTS

A comparison of the AL − SPL curves (Figures 40, 41, and 45) indicates that there is little agreement between the SI and SR tests as far as the responses at the base of the adapter truss, at the top of the adapter truss, and at the experiment panels are concerned. When Figures 42, 43, and 44 are examined, however, it is evident that the SI and SR tests agree favorably for the responses at the top of the spacecraft, at the solar arrays, and at the top of the folded EP-6 boom.

27

All three translational axes of measurement were included in the AL – SPL average curves; that is, the response curves are not unique to a particular axis. Figures 28 through 32 and Figures 34 through 38 demonstrate clearly the insignificant differences between the AL – SPL curves of the accelerometers measuring longitudinal motion (Y-axis) and those measuring transverse motion (X- and Z-axes).

The agreement of the responses at the top of the spacecraft, EP-6 boom, and solar arrays is also supported by the ratios of the overall accelerometer response (g_{rms}) given in Table 2. When the results from the eight accelerometers mounted at these three positions are compared, the SR test average is 98 percent of the SI test average. In comparison, the SR test ratios of the nine accelerometers mounted on the top and bottom of the spacecraft truss are only 55 percent of the SI values. The experiment-panel responses are so inconsistent for both the AL – SPL curves and overall g_{rms} comparisons that their response remains unpredictable.

It is extremely difficult to compare the PSD plots of corresponding accelerometer responses for the two tests; the sharpness of the peaks and the log-log plotting technique tend to distort the information and give undue emphasis to the lower-frequency levels. If these drawbacks are remembered when the PSD responses at the base of the adapter truss are noted for the SI and SR tests (Figures 10 and 15), some interesting observations may be made. The response, as a function of frequency, differs considerably in the two tests. In the SI test, the response peaks at about 100 and 800 Hz, whereas the SR test response is much more uniform. The G-versus-frequency plot (Figure 22) demonstrates this behavior much more clearly in that it shows a measure of the energy input to each particular one-third
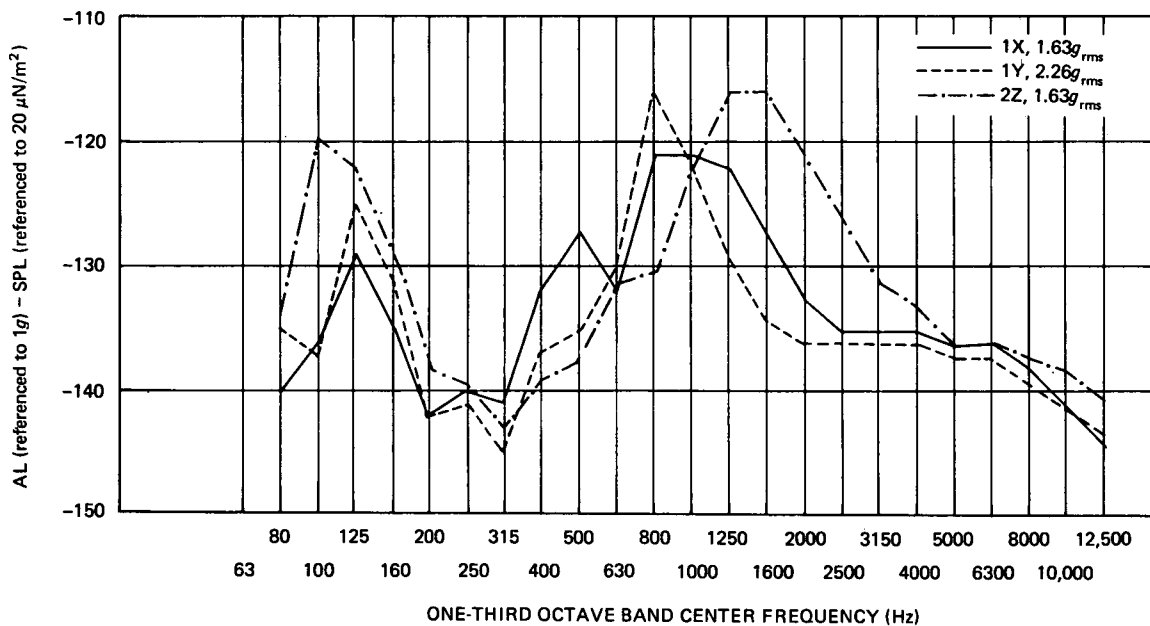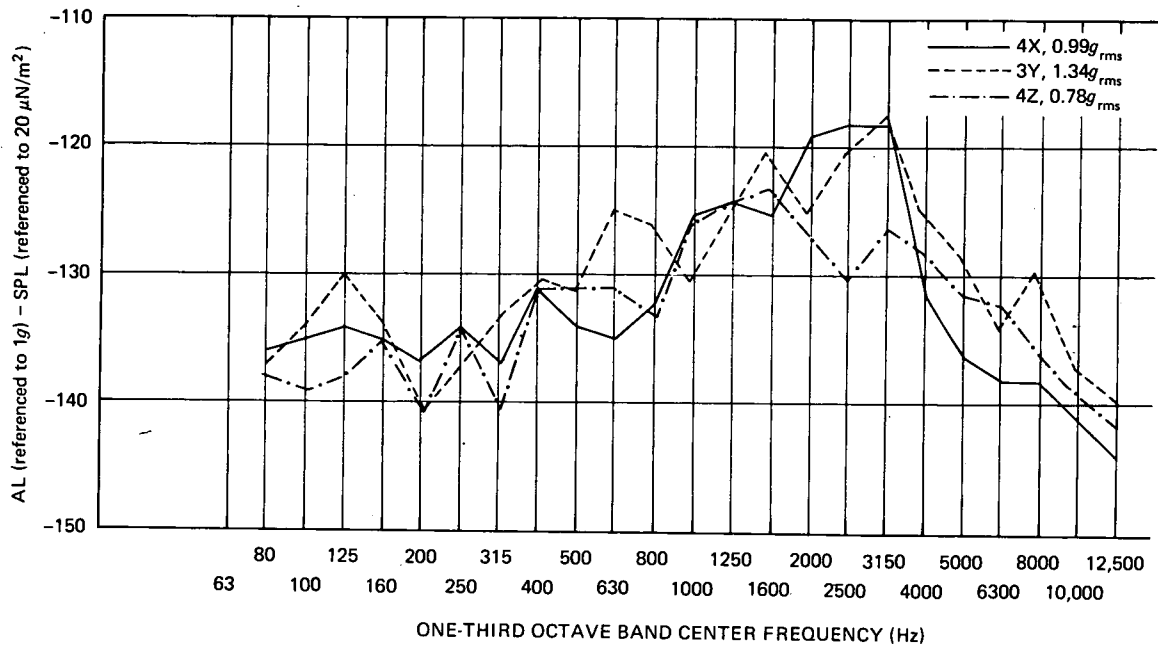

Figure 28. SI Test Acceleration Level, Base of Truss

28

Figure 29. SI Test Acceleration Level, Top of Truss
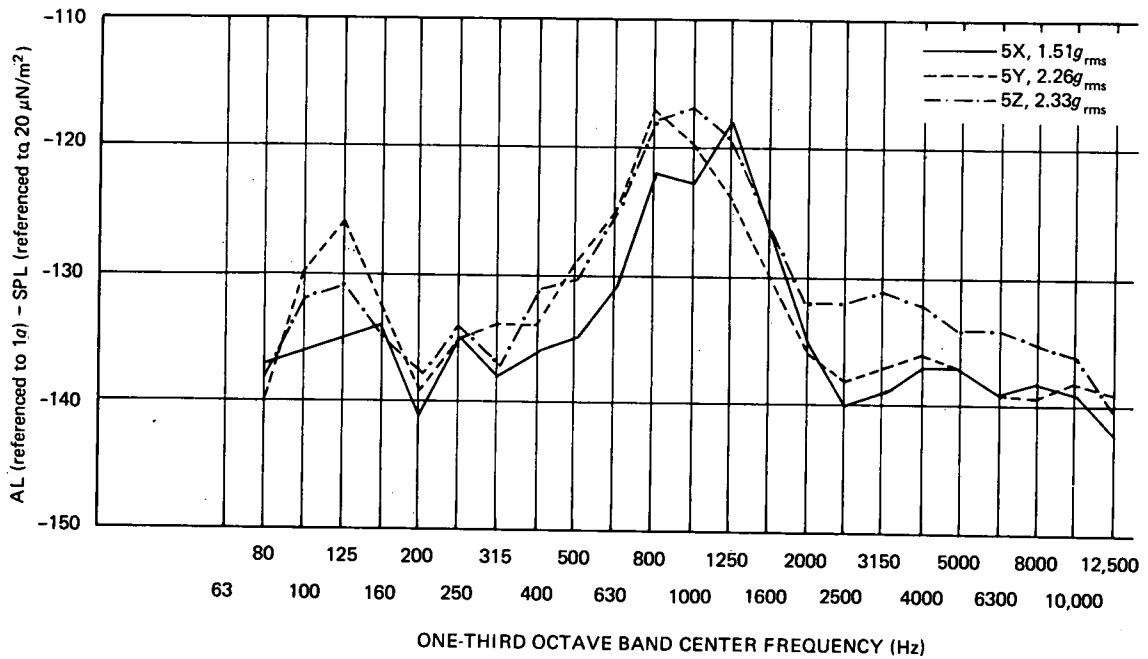

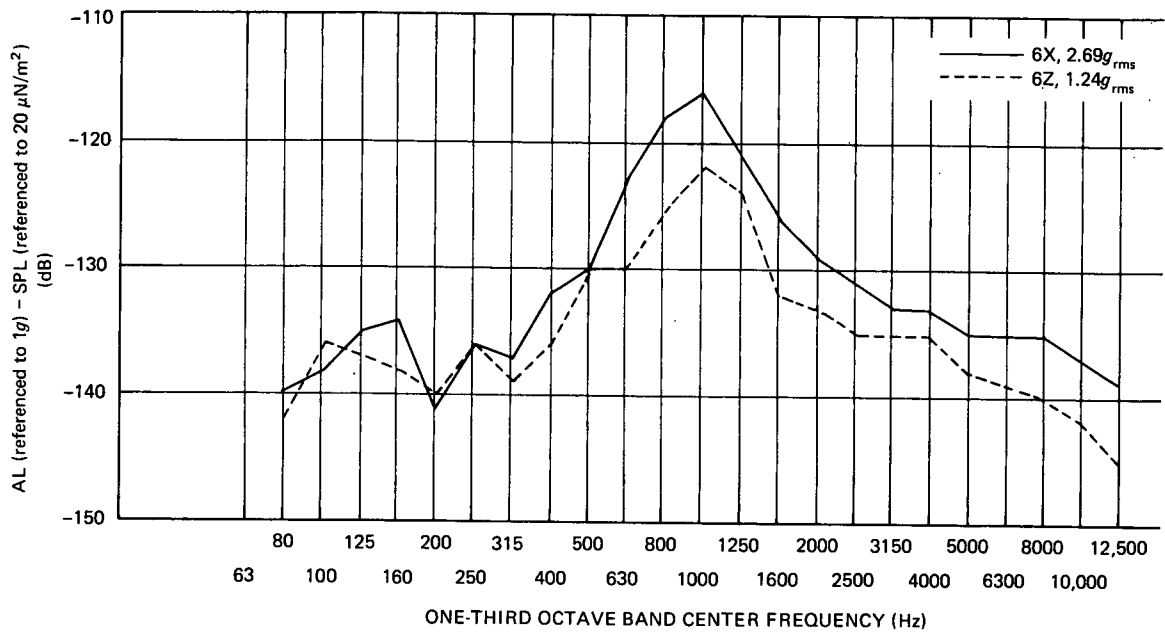**Figure 30. SI Test Acceleration Level, Top of Spacecraft**

Figure 31. SI Test Acceleration Level, Solar Array
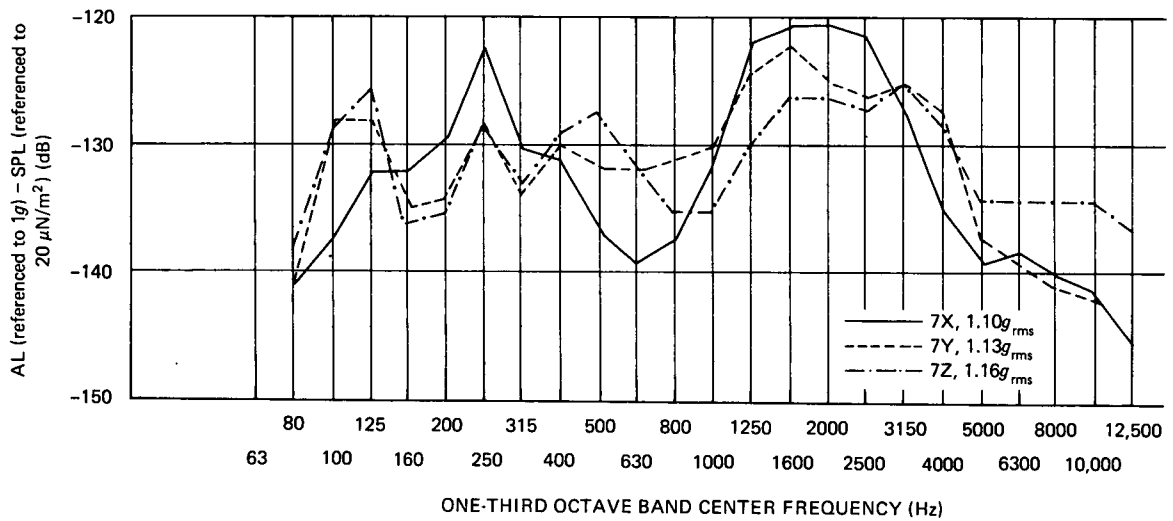

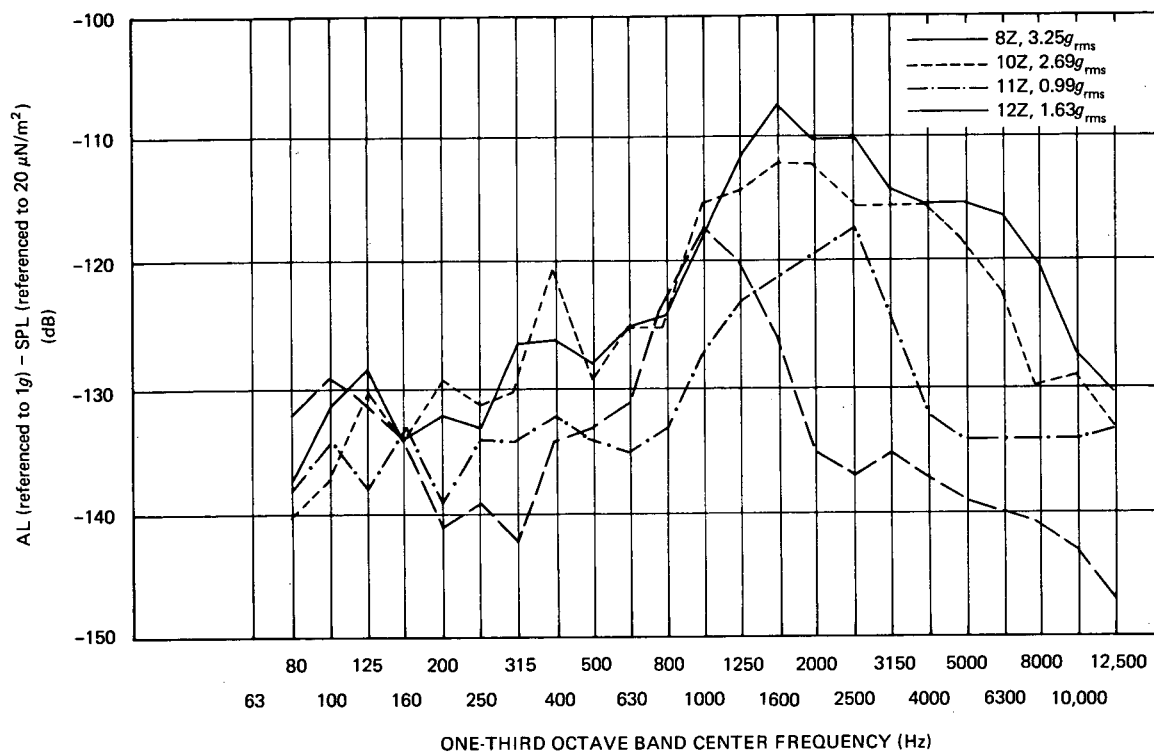Figure 32. SI Test Acceleration Level, EP-6 Boom

30

Figure 33. SI Test Acceleration Level, Experiment Panel
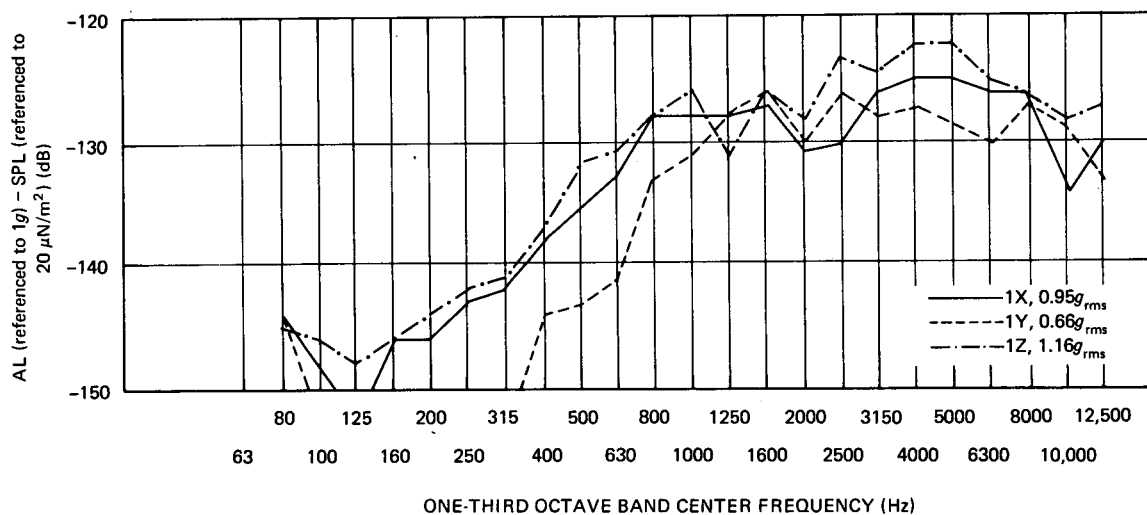

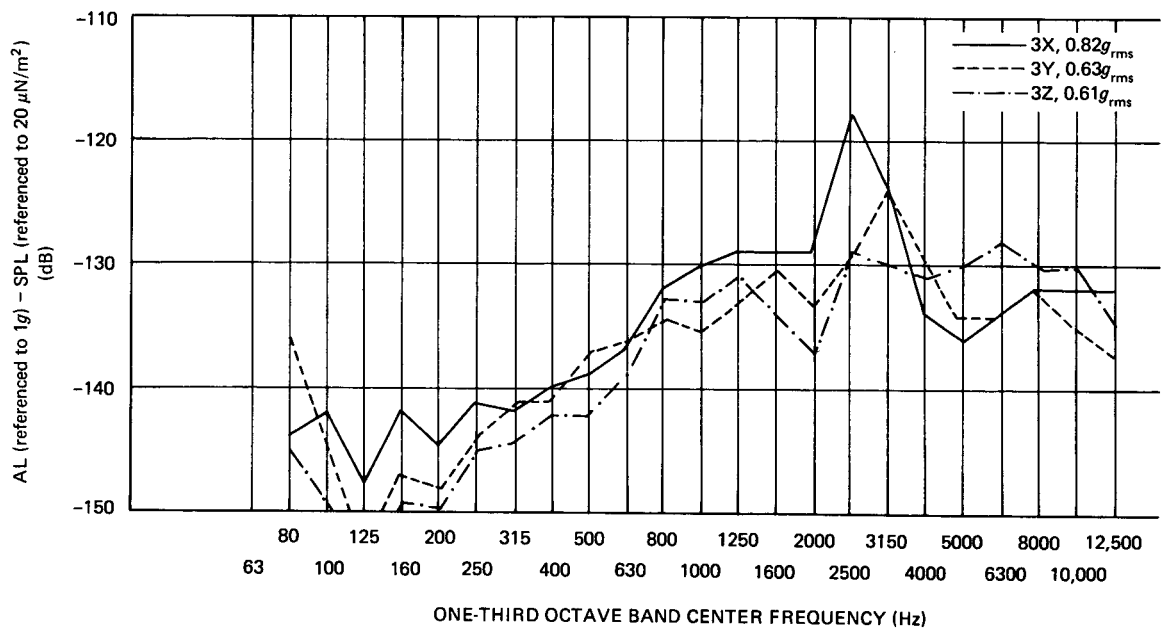Figure 34. SR Test Acceleration Level, Base of Truss

31

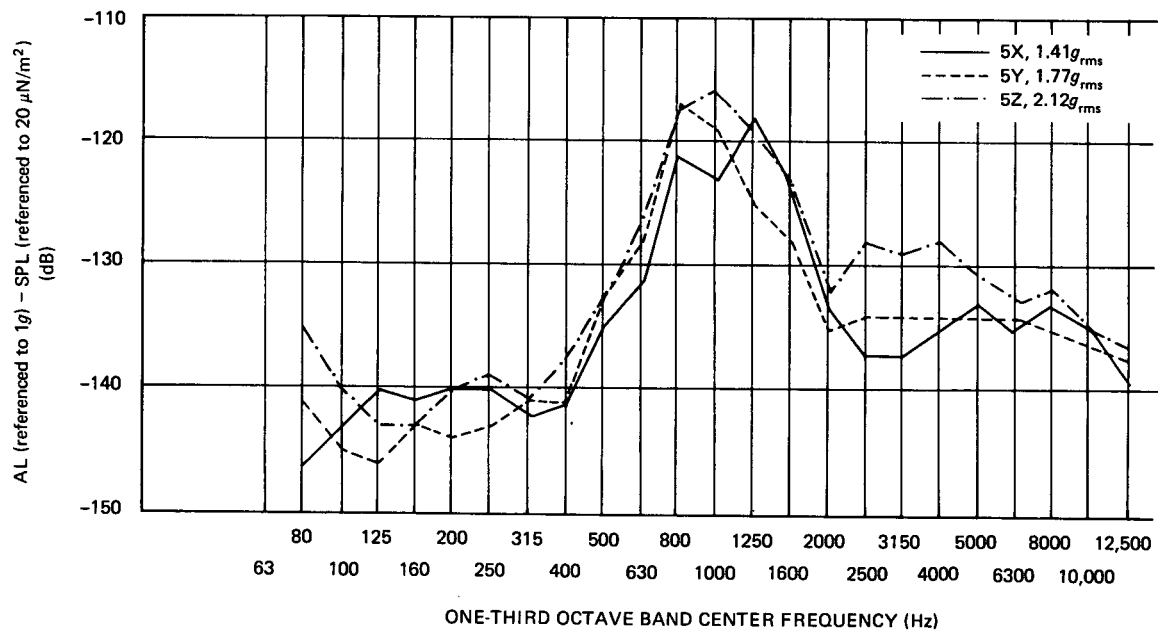Figure 35. SR Test Acceleration Level, Top of Truss

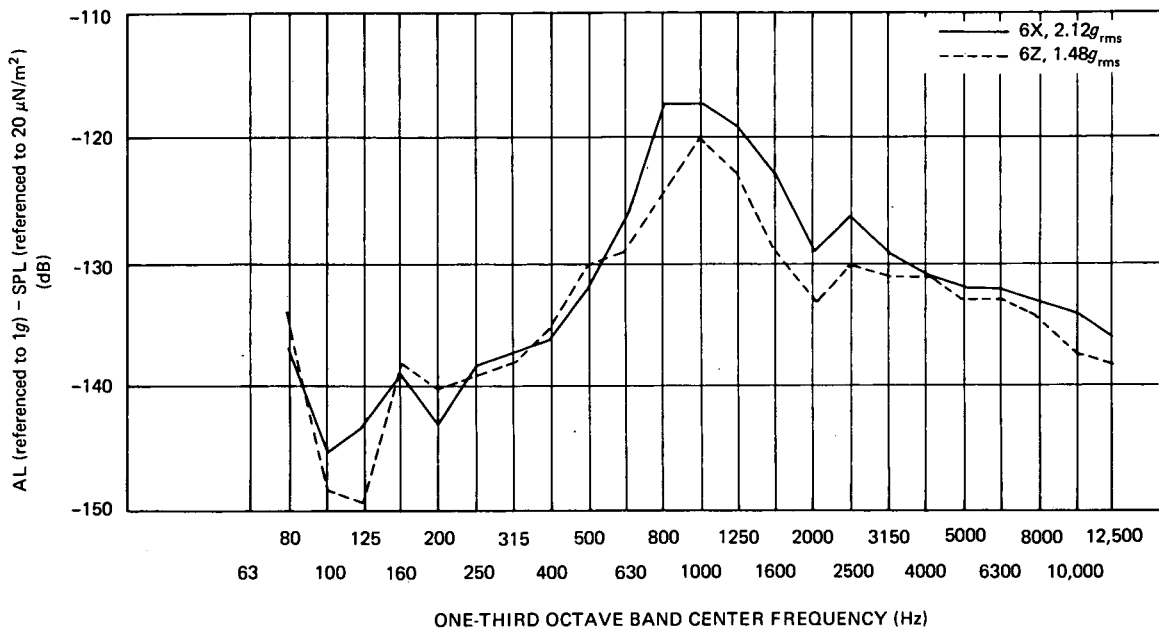Figure 36. SR Test Acceleration Level, Top of Spacecraft

32

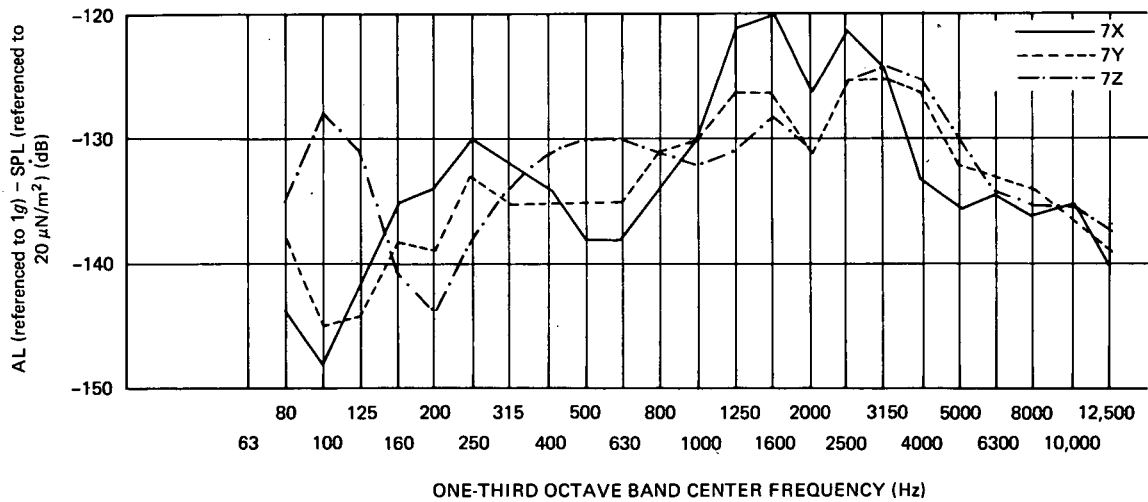Figure 37. SR Test Acceleration Level, Solar Array

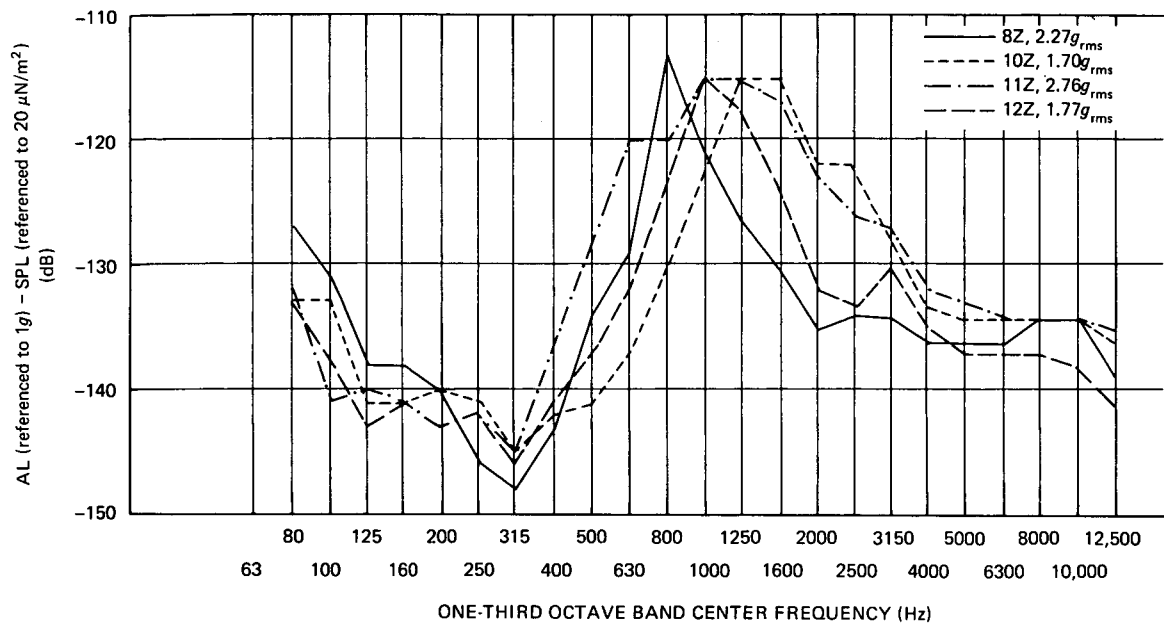Figure 38. SR Test Acceleration Level, EP-6 Boom

33

Figure 39. SR Test Acceleration Level, Experiment Panel

Figure 40. Comparison of SI and SR Test Average Acceleration Level, Base of Truss

34

Figure 41. Comparison of SI and SR Test Average Acceleration Level, Top of Truss

Figure 42. Comparison of SI and SR Test Average Acceleration Level, Top of Spacecraft

35
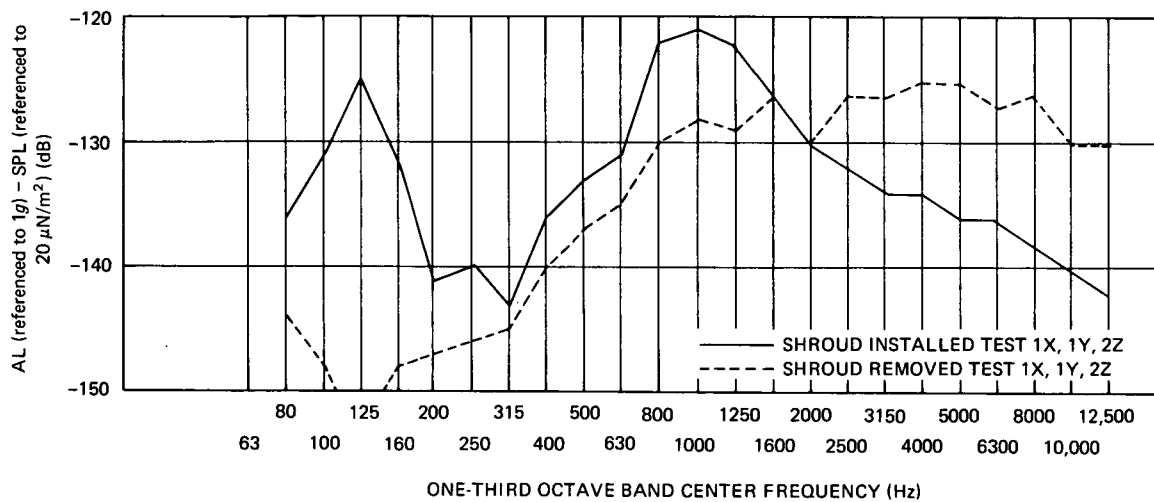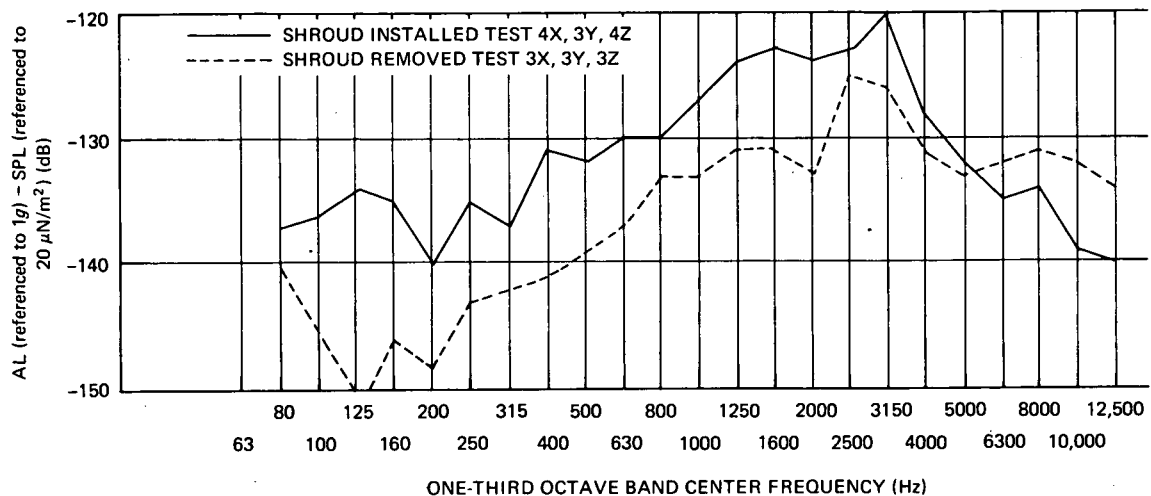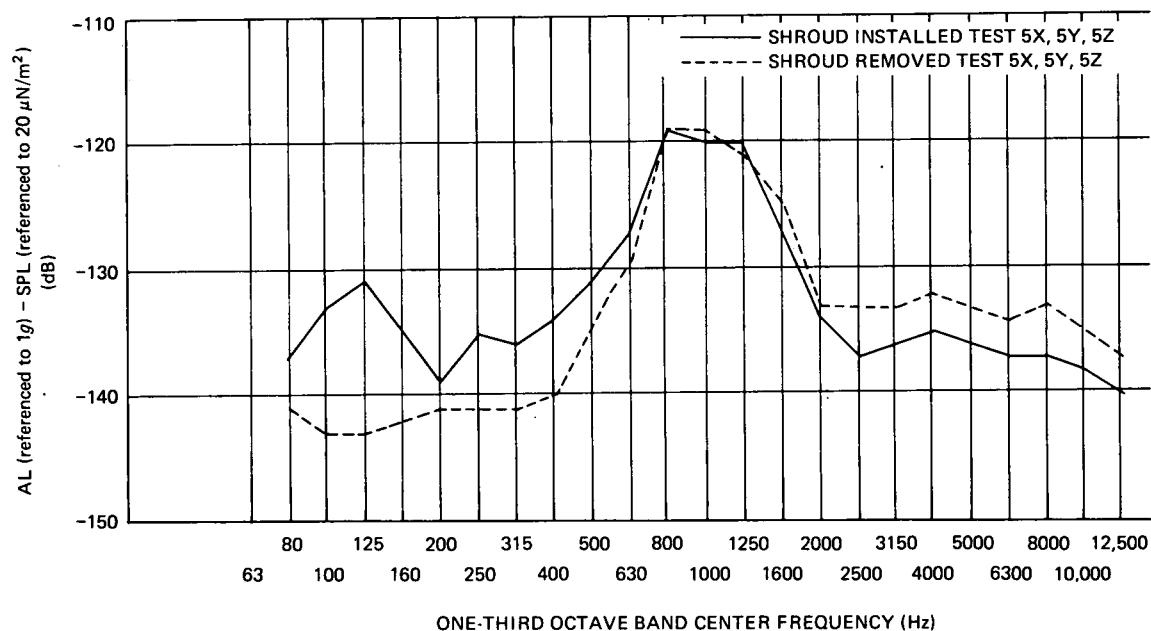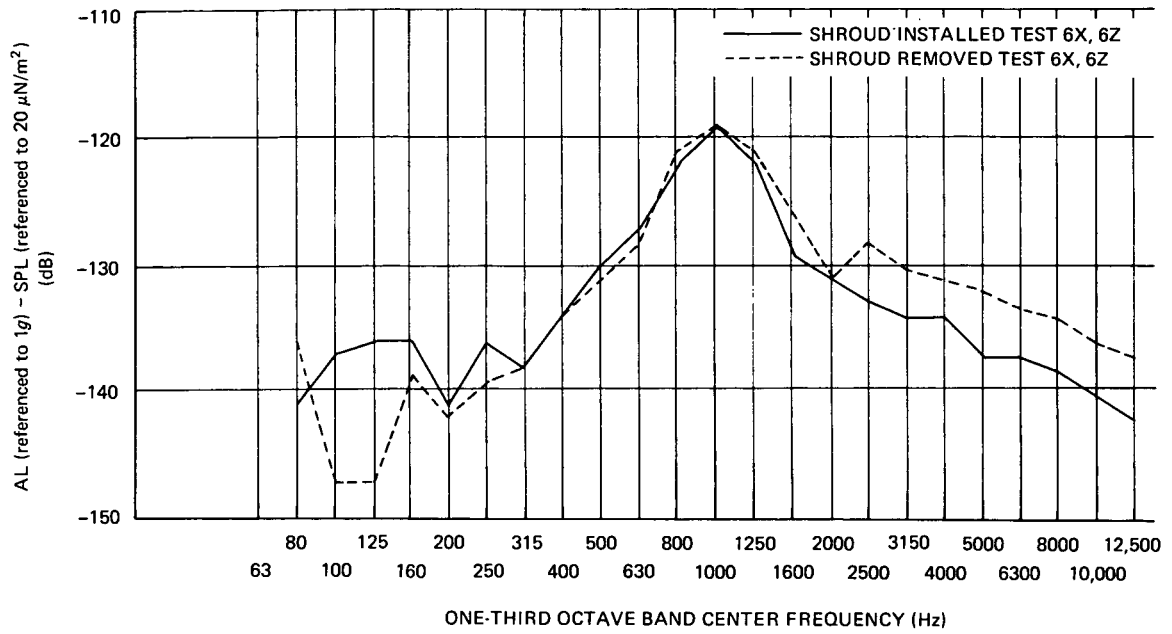
Figure 43. Comparison of SI and SR Test Average Acceleration Level, Solar Array
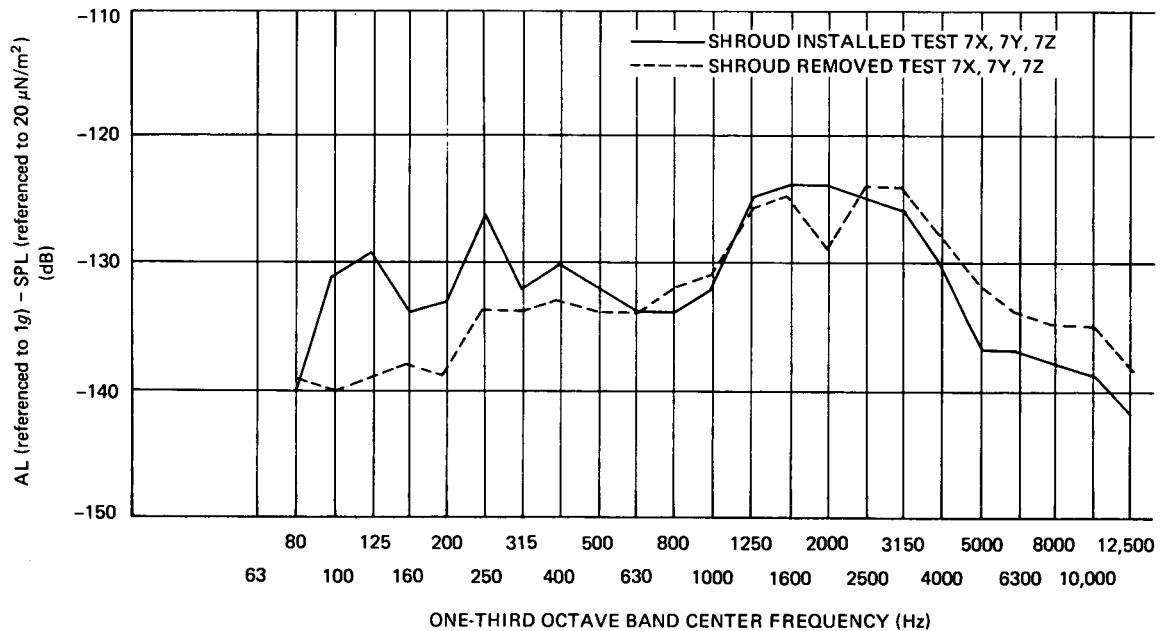

Figure 44. Comparison of SI and SR Test Average Acceleration Level, Top of Folded EP-6 Boom

36
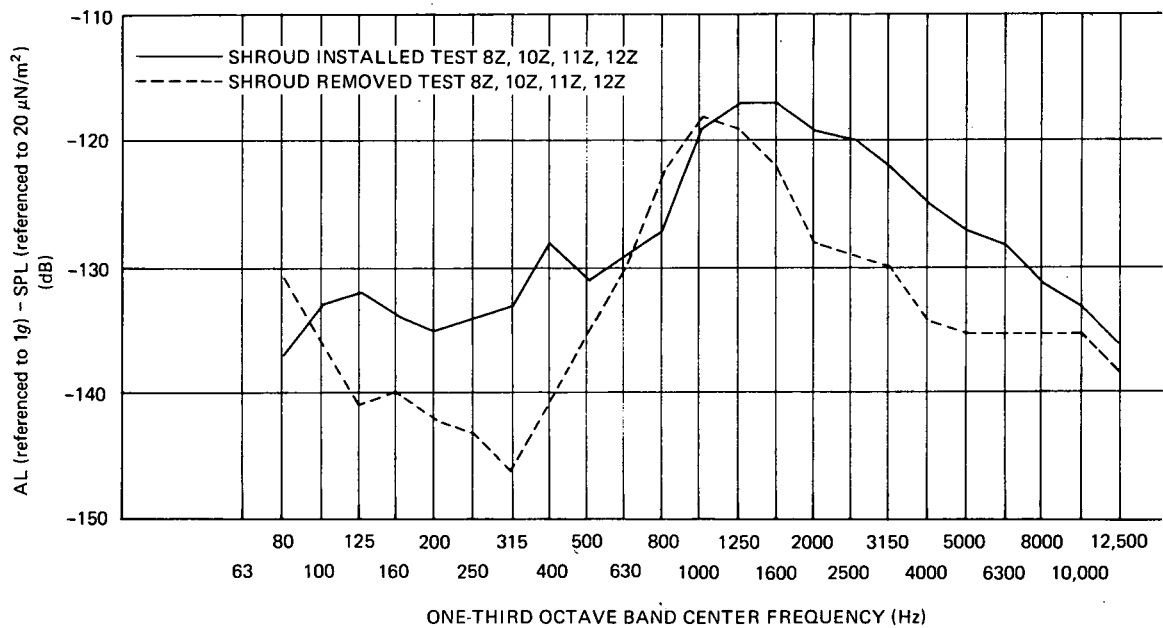
Figure 45. Comparison of SI and SR Test Average Acceleration Level, Experiment Panels

octave band for each test. For the SI test, the $g_i^2 / \Sigma g_i^2$ ratio totals 77 percent between 500 and 1250 Hz, whereas this ratio totals only 41 percent for the SR test.

Table 3 is presented as an aid to interpreting the PSD plots. It presents a summation of the G-values in the frequency bands from 63 to 400 Hz, 500 to 1250 Hz, and 1600 to 12 500 Hz for both tests, as taken from Figures 22 through 27.

TABLE 3
FREQUENCY RESPONSE DATA ($G \times 100$)

Accelerometer Locations	63 to 400 Hz		500 to 1250 Hz		1600 to 12 500 Hz	
	SI	SR	SI	SR	SI	SR
Base of truss	18.5	9.1	77.3	41.3	4.2	49.6
Top of truss	17.9	17.4	60.3	38.4	21.8	44.3
Top of spacecraft	5.8	5.6	92.8	89.5	1.4	4.9
Solar array	4.8	10.7	94.7	84.0	0.5	5.3
EP-6 boom	46.5	47.0	39.8	33.8	13.7	19.2
Experiment panels	16.2	4.5	55.4	83.6	29.0	11.9

These data indicate that, with the exception of the EP-6 boom response, the SI test responses fall primarily in the frequency range of 500 to 1250 Hz, with peaks at 800 Hz. They also demonstrate once again the good agreement between the solar-array response, the boom response, and the top-of-the-spacecraft response.

CONCLUSIONS

The results indicate that, in general, the shroud is necessary when conducting an acoustic test, unless it is possible to adjust the input levels to account for the absence of the shroud, in which case a considerable amount of flight data would be necessary. An acoustic test with shroud removed and with simulated internal acoustic inputs cannot otherwise duplicate the test responses with shroud installed and with external acoustic inputs, which would be the flight conditions.

In reference to the OGO structural model, tests with and without the shroud produced equivalent responses only at points distant from the spacecraft/adapter region, such as some locations on the top of the spacecraft, solar array, and EP-6 boom.

Although no concrete reasons can be given for the peaks in the response curve in the region of 500 to 1250 Hz, it is believed that they were caused by acoustic-field/spacecraft-structure coincidence frequencies.

Apparently, for this specific test article, a significant portion of the vibration response (SI condition) is caused by the acoustic excitation of the shroud, which in turn is transmitted through the spacecraft trusses via the mechanical path. The reduction in level when the shroud is removed (SR) indicates the total absence of acoustic energy that ordinarily would have traveled the mechanical path. Therefore the shroud is much more than an acoustic-attenuating device with an aerodynamic shape; it provides a mechanical energy path for undesired energy inputs to the spacecraft. The presence or absence of this path causes tests with and without the shroud to show significantly different results.

Future acoustic tests should be conducted with proper consideration given to simulation of the total shroud effects; only in this way can a worthwhile acoustic test be performed.

RECOMMENDATIONS

The acoustic tests described in this report provide answers to only a very small portion of the complex questions inherent in the acoustic test simulation field; much work remains to be done. The following list of research areas to be investigated is based on the results obtained from this test:

(1) Type of adapter—The present test employed a rigid adapter. Future tests should evaluate the effects on the energy flow along the mechanical path when a more elastic adapter is employed.

(2)   Reverberant field considerations—For the SR configuration, the LPS test chamber only approximates a reverberant field. A worthwhile test would be to test the spacecraft alone in a reverberant test chamber.

(3)   Transmission path study—Energy reaches the shroud-enclosed spacecraft via two paths, the acoustic path and the mechanical path. Knowledge of the relative importance of the two paths is of considerable value when considering simulation methods. A valuable study therefore would consist of isolating each path successively to determine the relative contribution of each path of energy input to the total spacecraft response.

(4)   Combined acoustic-vibratory environments—Future tests in the launch environment simulation area could also investigate the effects of supplementing the acoustic input to a spacecraft with vibratory mechanical inputs applied to the spacecraft adapter interface. The resulting acoustic-vibratory environment when applied to a spacecraft with the shroud removed might then be equivalent to testing a spacecraft with the shroud installed subjected only to an acoustic environment.

Performance of these recommended research tasks will provide valuable information necessary for the design of realistic acoustic simulation tests.

REFERENCES

1.   Kirchman, E. J., and Arcilesi, C. J., "Advanced Combined Environmental Test Facility," *The Shock and Vibration Bulletin* No. 37, Part 3, January 1968.

2.   Manning, Jerome E., and Maidanik, Gideon, "Radiation Properties of Cylindrical Shells," *The Journal of the Acoustical Society of America* 36(9):1691-1698, September 1964.

3.   Mitchell, R. S. and Dorian, R. A., "Dyvan User's Guide Release I," GSFC Memorandum Report No. 691-19, DIRS No. 01828, July 31, 1969.